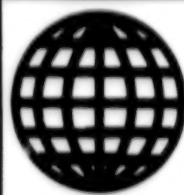


JPRS-UPM-92-001  
15 JANUARY 1992



**FOREIGN  
BROADCAST  
INFORMATION  
SERVICE**

---

# ***JPRS Report***

# **Science & Technology**

---

***Central Eurasia:  
Physics & Mathematics***

# Science & Technology

## Central Eurasia: Physics & Mathematics

JPRS-UPM-92-001

### CONTENTS

15 JANUARY 1992

**NOTICE TO READERS:** The name of this book will change from "USSR: Physics & Mathematics" to "Central Eurasia: Physics & Mathematics" as of 6 January 1992.

#### Acoustics

- Two-Phase Flows at Supersonic Velocities  
*[O. A. Povarov, V. A. Filippenko; TEPLOFIZIKA VYSOKIKH TEMPERATUR, Vol 29 No 4, Jul-Aug 91]* ..... 1
- Raman Scattering of Light in Degenerate (Pb,Sn)Se Semiconductor  
*[L. K. Vodopyanov, L. A. Falkovskiy, et al.; PISMA V ZHURNAL EKSPERIMENTALNOY I TEORETICHESKOY FIZIKI, Vol 53 No 11, 10 Jun 91]* ..... 1
- Evolution of Turbulence in Underexpanded Supersonic Jet  
*[S. A. Novopashin, A. L. Perepelkin; SIBIRSKIY FIZIKO-TEKHNICHESKIY ZHURNAL, No 1, Jan-Feb 91]* ..... 1

#### Crystals, Laser Glasses, Semiconductors

- Crystals of New Compound  $Cs_3H_3(SeO_4)_4 \cdot H_2O$  (CTSeM): Atomic Structure and Phase Transitions  
*[B. V. Merinov, A. I. Baranov, et al.; KRISTALLOGRAFIYA, Vol 36 No 3, May-Jun 91]* ..... 3
- Antiphase Interfaces in GaAs  
*[V. I. Vdovin, M. G. Milvidskiy, et al.; KRISTALLOGRAFIYA, Vol 36 No 3 May-Jun 91]* ..... 3
- Characteristics of Defect Formation in Active Region of GaAlAs/GaAs Epitaxial Heterostructures for Solar Cells During Heating-Cooling Cycles  
*[A. A. Kalinin, M. G. Milvidskiy, et al.; KRISTALLOGRAFIYA, Vol 36 No 3, May-Jun 91]* ..... 3
- Nanosecond Switching in Submicron-Size Sandwich Structures With Amorphous  $Ge_xTe_{1-x}$  Film  
*[E. Babenskas, S. Balevicius, et al.; LITOVSKIY FIZICHESKIY SBORNIK, Vol 31 No 3, May-Jun 91]* ..... 4
- Impact Ionization of Shallow Donors in n-InP Layers  
*[A. Dargys, J. Kundrotas, et al.; LITOVSKIY FIZICHESKIY ZHURNAL, Vol 31 No 3, May-Jun 91]* ... 4
- Effect of Electron Irradiation on Electric Properties and Photoluminescence of Nuclei-Doped Gallium Arsenide  
*[V. N. Brudnyy, D. L. Budnitskiy, et al.; IZVESTIYA VYSSHIKH UCHEBNYKH ZAVEDENIY: FIZIKA, Vol 34 No 4, Apr 91]* ..... 5
- Effect of Electron Irradiation on Germanium-Doped Gallium Arsenide Properties  
*[V. N. Brudnyy, D. L. Budnitskiy, et al.; IZVESTIYA VYSSHIKH UCHEBNYKH ZAVEDENIY: FIZIKA, Vol 34 No 4, Apr 91]* ..... 5
- Hall EMF in Compensated Semiconductors and Semimetals  
*[V. A. Kozlov, K. A. Sakharov; FIZIKA TVERDOGO TELA, Vol 33 No 4, Apr 91]* ..... 6

#### Lasers

- Parametric Emission and Phase Conjugation of Intersecting Laser Beams in Nematic Liquid-Crystal Layer With Dye  
*[O. L. Animonov, N. A. Dvoryaninov, et al.; PISMA V ZHURNAL EKSPERIMENTALNOY I TEORETICHESKOY FIZIKI, Vol 53 No 12, 25 Jun 91]* ..... 7
- Photoelectron Emission by Surfaces of Materials Exposed to Short-Wave Radiation  
*[O. B. Ananin, Yu. A. Bykovskiy, et al.; PISMA V ZHURNAL TEKHNICHESKOY FIZIKI, Vol 17 No 12, 26 Jun 91]* ..... 7
- Auger-Transition 108.9 nm Xe-Laser Pumped by "Atomic" Bremsstrahlung From Proton Beam  
*[A. D. Andreyev, V. V. Ryzhov; PISMA V ZHURNAL TEKHNICHESKOY FIZIKI, Vol 17 No 12, 26 Jun 91]* ..... 8
- Threshold Characteristics of Laser With Nuclear Pumping of Transitions in Xe-Atom  
*[S. P. Melnikov, A. A. Sinyanskiy; PISMA V ZHURNAL TEKHNICHESKOY FIZIKI, Vol 17 No 12, 26 Jun 91]* ..... 8

Amplitude and Frequency Characteristics of Double-Mode Ring Lasers With Controllable Phase Anisotropy [V. I. Timofeyev; KVANTOVAYA ELEKTRONIKA, Vol 18 No 6, Jun 91]	9
Dynamics of Spectral and Angular Excimer-Laser Radiation Emission Characteristics [A. G. Zhidkov, A. O. Tersikh, et al.; KVANTOVAYA ELEKTRONIKA, Vol 18 No 6, Jun 91]	9
Radiation Emission Characteristics of Pulsed CO <sub>2</sub> -Laser in Unstable Optical Cavity With Nonuniform-Reflectance Exit Mirror [M. N. Kuznetsov, O. L. Kulikov; KVANTOVAYA ELEKTRONIKA Vol 18 No 6, Jun 91]	10
Flow Patterns Resulting From Interaction of Twin CO <sub>2</sub> -Laser Pulses and Target in Air [A. A. Bakeyev, L. I. Nikolashina, et al.; KVANTOVAYA ELEKTRONIKA, Vol 18 No 6, Jun 91]	10
Feasibility of Picosecond Terawatt Nd-Laser With About 10 <sup>13</sup> :1 Contrast Ratio [L. L. Losev, A. P. Lutsenko, et al.; KVANTOVAYA ELEKTRONIKA, Vol 18 No 5, May 91]	11
New Laser Crystal Emitting Dark-Red Radiation at 300 K Temperature [A. A. Kaminskiy, A. G. Petrosyan; KVANTOVAYA ELEKTRONIKA, Vol 18 No 5, May 91]	11
Pulsed Laser ISKRA-5 With 120 TW Power Rating [V. I. Annenkov, V. A. Bagretsov, et al.; KVANTOVAYA ELEKTRONIKA, Vol 18 No 5, May 91]	12
Electric-Discharge Excimer XeCl-Laser Generating Long Emission Pulse [V. V. Atezhov, V. S. Bukreyev, et al.; KVANTOVAYA ELEKTRONIKA, Vol 18 No 5, May 91]	12
New Class of Solitons in Optical Fibers Near Zero-Dispersion Point [V. K. Mezentshev, S. K. Turitsyn; KVANTOVAYA ELEKTRONIKA, Vol 18 No 5, May 91]	13
Characteristics of Multichannel-Laser Radiation Pattern Formation by Beam Focusing [S. Yu. Denison, Ye. V. Zelenov; KVANTOVAYA ELEKTRONIKA, Vol 18 No 5, May 91]	13
Experimental Detection of Plasma Wave Barrier Brightening by Electron Beam [I. A. Anisimov, S. M. Levitskiy, et al.; ZHURNAL TEKHNIЧЕСКОY FIZIKI, Vol 61 No 3, Mar 91]	14

## Nuclear Physics

Dibaryons and Thresholds [I. I. Starkovskiy; FIZIKA ELEMENTARNYKH CHASTITS I ATOMNOGO YADRA, Vol 22 No 3, May-Jun 91]	15
Comparison Between Complete Systems of Levels in <sup>108-116</sup> Cd, <sup>114-124</sup> Sn, <sup>122-130</sup> Te Isotopes up to 2.5-3.0 MeV Excitation Energy [A. M. Demidov, I. V. Mikhaylov; YADERNAYA FIZIKA, Vol 53 No 5, May 91]	15
Dynamics of Nonlinear-Schrodinger-Equation Soliton in Uniform Field in Adiabatic Approximation [A. G. Lavkin; YADERNAYA FIZIKA, Vol 53 No 5, May 91]	15
New Approach to Treatment of Pontekorvo Reactions [A. B. Kaydalov; YADERNAYA FIZIKA, Vol 53 No 5, May 91]	16
Measurement of Cross-Sections for Interaction of Reactor Antineutrino and Deuteron in Rovno Nuclear Electric Power Plant [A. G. Vershinskiy, A. A. Meluzov, et al.; PISMA V ZHURNAL EKSPERIMENTALNOY I TEORETICHESKOY FIZIKI, Vol 53 No 10, 25 May 91]	16
Deformation of <sup>74-80</sup> Kr Nuclei and Their Moments of Inertia [I. Kh. Lemberg, I. A. Mitropolskiy; IZVESTIYA AKADEMII NAUK SSSR: SERIYA FIZICHESKAYA, Vol 55 No 1, Jan 91]	17

## Optics, Spectroscopy

Propagation of Light Pulse Through Tunnel-Coupled Nonlinear Optical Waveguides [A. I. Maymistov; KVANTOVAYA ELEKTRONIKA, Vol 18 No 6, Jun 91]	18
Luminescence of Absorption Domains (Autowaves) in CdS [V. A. Stadnik; PISMA V ZHURNAL EKSPERIMENTALNOY I TEORETICHESKOY FIZIKI, Vol 53 No 10, 25 May 91]	18
Change in Optical Properties of Leucosapphire Caused by Hot Plastic Deformation [I. I. Afanasyev, L. K. Andrianova, et al.; FIZIKA TVERDOGO TELA, Vol 33 No 4, Apr 91]	18
Optical Waveguide Electrooptic RF Field Transducer [V. K. Gorchakov, V. V. Kutsayenko, et al.; ZHURNAL TEKHNIЧЕСКОY FIZIKI, Vol 61 No 3, Mar 91]	19
Fiber Optic Sensor For Magnetic Field Transducer [S. N. Antonov; ZHURNAL TEKHNIЧЕСКОY FIZIKI, Vol 61 No 3, Mar 91]	19

## Plasma Physics

Production of Hot Electrons in Open Traps During Electron-Cyclotron-Resonance Heating With Longitudinal Injection of Microwave Power [V. A. Zhiltsov, A. A. Skovoroda, et al.; <i>FIZIKA PLAZMY</i> , Vol 17 No 7, Jul 91]	20
Anomalous Large Cathode Region in Molecular High-Pressure Plasma [S. Ya. Bronin, A. A. Vanin; <i>FIZIKA PLAZMY</i> , Vol 17 No 7, Jul 91]	20
Anomalous Plasma Transport in Neoclassical Modes Due to Pressure Gradient [V. P. Lakhin; <i>FIZIKA PLAZMY</i> Vol 17 No 6, Jun 91]	21
Limitation of Microwave Radiation Pulse Duration in Oscillators With Microsecond-Pulse Relativistic Electron Beams [S. N. Voronkov, O. T. Loza, et al.; <i>FIZIKA PLAZMY</i> , Vol 17 No 6, Jun 91]	21
Formation of Wide High-Current Electron Beam of Microsecond Duration [E. N. Abdullin, S. Ya. Belomytsev, et al.; <i>FIZIKA PLAZMY</i> , Vol 17 No 6, Jun 91]	22
Maximum Electric Field Intensity in Plasma Wake Wave [S. V. Bulanov, V. I. Kirsanov, et al.; <i>PISMA V ZHURNAL EKSPERIMENTALNOY I TEORETICHESKOY FIZIKI</i> , Vol 53 No 11, 10 Jun 91]	22
Development of Diffusion Processes During Plasma-Arc Deposition of Coatings [S. A. Rebun, A. P. Kudinov; <i>SIBIRSKIY FIZIKO-TEKHNICHESKIY ZHURNAL</i> , No 1, Jan-Feb 91]	23

## Superconductivity

Acoustic Spectrum Modification of Piezocrystal Wafers Using Superconducting and Metallic Coats [V. I. Alshits, V. N. Lyubimov; <i>KRISTALLOGRAFIYA</i> , Vol 36 No 4, Jul-Aug 91]	24
Steady-State Josephson Effect in High- $T_c$ Superconductor Junctions [B. A. Aminov, L. Roshta, et al.; <i>FIZIKA NIZKIKH TEMPERATUR</i> , Vol 17 No 6, Jun 91]	24
High-Temperature Quantum Interferometer [V. V. Kartsovnik, P. P. Pavlov, et al.; <i>FIZIKA NIZKIKH TEMPERATUR</i> , Vol 17 No 6, Jun 91]	24
Anomalous Thermodynamic Characteristics of S-N Superlattice [A. I. Buzdin, V. P. Damjanovich, et al.; <i>PISMA V ZHURNAL EKSPERIMENTALNOY I TEORETICHESKOY FIZIKI</i> , Vol 53 No 10, 25 May 91]	25
Electron Paramagnetic Resonance in (Er,Y)-Ba-Cu-O System [A. G. Anders, S. V. Volotskiy, et al.; <i>FIZIKA NIZKIKH TEMPERATUR</i> , Vol 17 No 5, May 91]	25
Formation of 2234-Phase in Bi-Sr-Ca-Cu-O Films Doped With Pb and Sb [L. S. Palatnik, A. L. Toptygin, et al.; <i>FIZIKA NIZKIKH TEMPERATUR</i> , Vol 17 No 5, May 91]	26
Microwave Absorption by Type-II Superconductors in Magnetic Field [S. N. Lukin, O. P. Teslya, et al.; <i>FIZIKA NIZKIKH TEMPERATUR</i> , Vol 17 No 5, May 91]	27
Raman Spectroscopy of $\text{CsMnCl}_3 \cdot 2\text{H}_2\text{O}$ Crystal [V. P. Gnezdilov, V. V. Yermenko, et al.; <i>FIZIKA NIZKIKH TEMPERATUR</i> , Vol 17 No 5, May 91]	27
Microwave Absorption by High- $T_c$ Superconductor Ceramic in Magnetic Field [V. V. Kveder, M. R. Mkrtchyan, et al.; <i>FIZIKA TVERDOGO TELA</i> , Vol 33 No 4, Apr 91]	28

## Thermodynamics

Speed of Sound in Primary Normal Liquid Alcohols [T. S. Khasanshin; <i>TEPLOFIZIKA VYSOKIKH TEMPERATUR</i> , Vol 29 No 4, Jul-Aug 91]	29
Thermodynamic Functions of Three-Dimensional Ising Model Near Phase Transition Point Allowing for Scaling Corrections. II. $TT_c$ Case [M. P. Kozlovskiy, I. V. Pylyuk, et al.; <i>TEORETICHESKAYA I MATEMATICHESKAYA FIZIKA</i> , Vol 87 No 3, Jun 91]	29

### Two-Phase Flows at Supersonic Velocities

927J0062B Moscow *TEPLOFIZIKA VYSOKIKH TEMPERATUR* in Russian Vol 29 No 4, Jul-Aug 91 pp 738-744

[Article by O. A. Povarov, V. A. Filippenko, Moscow Energy Institute]

UDC 532.529

[Abstract] The importance of examining two-component and two-phase flows at supersonic velocities for understanding the interaction of turbine blade metal with solid and liquid particles moving in the supersonic air or steam flow is emphasized. The behavior of the flow's liquid phase in the zone behind the shock wave is investigated; in so doing, the dimensions and velocity of liquid particles are taken into account in calculating the erosion wear rate of the turbine blade leading edge. Measurement data on changes in the dispersion composition of wet steam behind the shock wave at various flow velocities are cited. It is demonstrated that the sample erosion wear rate decreases in the supersonic flow of wet steam due to the breakup of liquid particles in the shock wave. Solid particles with a 10-200  $\mu\text{m}$  diameter made from materials with a 0.5-8.6  $\text{g/cm}^3$  density were used in the experiments. The results show that critical values of the Weber number for the liquid phase breakup in a wet steam stream in the shock waves fall within the 60-80 range. In order to decrease the erosion wear in a supersonic flow of droplets with a close to 0.4  $\mu\text{m}$  size, the leading edge must be at least 1.5 mm thick. Figures 7; references 14: 11 Russian, 3 Western.

### Raman Scattering of Light in Degenerate (Pb,Sn)Se Semiconductor

927J0022B Moscow *PISMA V ZHURNAL EKSPERIMENTALNOY I TEORETICHESKOY FIZIKI* in Russian Vol 53 No 11, 10 Jun 91 pp 561-565

[Article by L. K. Vodopyanov, Institute of Physics imeni P. N. Lomonosov, USSR Academy of Sciences, Moscow, L. A. Falkovskiy, Institute of Theoretical Physics imeni L. D. Landau, USSR Academy of Sciences, Moscow, G. Irvin and S. Khimenis, Simon Fraser University, Burnaby (Canada)]

[Abstract] An experimental study of Raman scattering of light in  $\text{Pb}_{1-x}\text{Sn}_x\text{Se}$  semiconductor crystals with  $x = 0.07-0.42$  was made, Raman spectroscopy of these crystals being made difficult by their opaqueness to laser radiation and small effective cross-section for its scattering but also by a high carrier concentration. Measurements were made with a computer-controlled laboratory Raman spectrometer in the backscattering configuration, weakly scattered light being recorded in a multi-channel optical analyzer with an ITT F4146 "Mepsicron" signal storage. The entire scattering spectrum was recorded simultaneously in 1000 channels of a micro-channel plate with a position-sensitive resistive anode.

This apparatus yielded very reliable data, operating with an ultralow dark current of approximately 0.05 counts/s and with a signal-to-noise ratio approximately 1000 times higher than attainable with a standard single-channel apparatus. A triple monochromator consisting of holographic diffraction gratings was built according to the "dispersion subtraction" scheme for elimination of scattered light of wavelengths close that of the excitation line. Resonance amplification, ensured by pumping a crystal with light of a wavelength corresponding to an energy close to the energy of an electron transition in the semiconductor molecule, intensified the signal sufficiently far above the noise level. As the excitation source was accordingly used a green (514.5 nm)  $\text{Ar}^+$ -laser, closely matching the 2.4 eV electron transition at the L-point in the energy band structure of such a semiconductor. Measurements were made at 16 K and 300 K temperatures with polarized pumping light and without polarization of the scattered light. The spectrum of a  $\text{Pb}_{0.93}\text{Sn}_{0.07}\text{Se}$  crystal was found to contain two wide peaks about 85  $\text{cm}^{-1}$  and 150  $\text{cm}^{-1}$  at 16 K. Its spectrum at 300 K was found to be smoother, with the intensity of scattered light decreasing from its highest level at the long-wave edge to its lowest level at the short-wave edge. A survey of elementary excitations in such a crystal reveals that such a Raman spectrum cannot be attributed to phonons, their frequencies in such a crystal being  $\omega_{\text{TO}} = 44 \text{ cm}^{-1}$  and  $\omega_{\text{LO}} = 140 \text{ cm}^{-1}$  according to earlier measurements made by the neutron diffraction method (V.K. Vodopyanov, I.V. Kucharenko, A.P. Shotov, and R. Scherm; *ZHURNAL EKSPERIMENTALNOY I TEORETICHESKOY FIZIKI* Vol 27, 1978). Neither is such a Raman spectrum attributable to plasmons or polaritons, their frequencies calculated on the basis of the applicable dispersion equation indicating that these excitations do not even occur within the range of that spectrum. Electronic excitations, whose properties depend largely on the ratio of length of mean free path  $\zeta$  for charge carriers to length of electromagnetic-field variation  $\lambda \approx 100 \text{ nm}$  in the crystal, can give rise to such a Raman spectrum: scattering by diffusons when  $\zeta \ll \lambda$  and scattering by electron-hole pairs when that ratio is large. This is demonstrated by theoretical analysis leading to a general expression for the intensity of scattered light and by subsequent calculation of the latter, assuming a refractive index  $n = 5.3$  for light of the  $\lambda = 514.5 \text{ nm}$  light. Figures 2; references 7.

### Evolution of Turbulence in Underexpanded Supersonic Jet

927J0042A Novosibirsk *SIBIRSKIY FIZIKO-TEKHNICHESKIY ZHURNAL* in Russian No 1, Jan-Feb 91 pp 89-95

[Article by S. A. Novopashin and A. L. Perepelkin, Institute of Thermophysics, Siberian Department, USSR Academy of Sciences, Novosibirsk]

UDC 535.6.001:535.5.517.4

[Abstract] An experimental study of a not fully expanded jet was made concerning the evolution of flow turbulence at its boundary within the range of laminar-to-turbulent transition. Precise contactless measurements based on Rayleigh scattering of light were made with the aid of pulsed laser radiation. A nitrogen jet was discharged from a sonic nozzle into a gaseous medium under very low pressure, the ratio of jet pressure to ambient pressure being sufficiently high for formation of "barrel" shock waves and an eddy layer along the nominal jet boundary. The quiescent stream was confined laterally by the pendant barrel-like compression front and ahead of it by a Mach disk, laminar-to-turbulent transition of flow in the eddy layer corresponding to the 1000-10,000 range of the Reynolds number  $N_{Re} = LV_m/\nu_{My}$  ( $L$  - distance from Mach disk,  $V_m$  - maximum jet velocity at exit from nozzle,  $\nu$  - kinematic viscosity of ambient gas). The nitrogen concentration in the eddy layer was measured with laser pulses of 20 mJ energy and 20 ns duration, the number of scattered photons being sufficiently large for the required accuracy of their count in small volumes of the order of  $1 \times 10^{-6} \text{ cm}^3$ . The apparatus included a pair of YAG lasers, each with a single amplifier stage followed by a nonlinear crystal acting as frequency doubler and a filter for extraction of 540 nm second-harmonic radiation. Each laser was triggered by a pulse from a separate G5-54 generator, both generators being controlled by a computer and the time difference between pulses of a pair being varied over the 0-1 ms range. One fraction of the 540 nm light extracted from each of the two laser beams was diverted for use as reference and recorded by an FD-256 photodiode, another fraction being diverted to another FD-256 photodiode whose electric output pulses triggered a G5-67 generator of synchronizing pulses. The remainders of the two light beams were reflected twice, first each by a separate plane mirror slanted at a 45° angle and then both by a common plane mirror, before a common lens focused them through an entrance window into the gas chamber (focal spot 0.1 mm in diameter, 1 cm long caustic) with an exit window

diametrically on the opposite side. The distance between the two caustics could be varied over the 0-2 mm range by varying the geometry of convergence of the two entering light beams. Parasitic reflections of light by the inside wall surface of the chamber were suppressed by black shields. Into the chamber were inserted two tubes, through two diametrically opposite lateral windows, each tube holding a Helios-40-2 objective (focal length 85 mm) which formed images of the caustics in the plane of a slot diaphragm behind it and an FEU-84 photomultiplier behind that diaphragm for recording the scattered light. The diaphragm behind one of the objectives was movable along the optical axis, for alignment with various points along the caustics. The output signals from the recording two photodiodes and two photomultipliers were sent to charge-code converters with a  $2.5 \times 10^{-13} \text{ C}$  sensitivity threshold, which integrated the input current from the respective photodevice with respect to time over the 300 ns duration of a synchronizing pulse. The converters in turn sent digital signals to a CAMAC crate for processing and analysis. The measurements revealed a breaking of the axial symmetry of flow and formation of a lobate flow pattern owing to development of a Gertler instability due to curvilinearity of flux tubes along the jet boundary, or Taylor instability due to flow of a denser gas along a path with a smaller radius of curvature in the field of centripetal forces, or instability associated with a positive pressure gradient in the compression region, but not possibly by an instability associated with inflection of the velocity profile. On the basis of the data obtained in this experiment have been established simultaneous spatial correlations in all three cylindrical coordinates at various instants of time and one-point time correlations at various points in space. With the aid of the respective correlation functions have then been calculated the fluctuation spectra characterizing development of turbulence. Regions of coherent flow, readily identifiable large-scale formations, were studied visually by the laser "knife" method and lobate formations found to develop during turbulent flow with Reynolds numbers  $N_{Re} > 100,000$  under conditions depending on the degree of surface roughness of the nozzle edge. Figures 7; references 9.

**Crystals of New Compound  $\text{Cs}_3\text{H}_3(\text{SeO}_4)_4 \cdot \text{H}_2\text{O}$  (CTSeM): Atomic Structure and Phase Transitions**

927J0038A Moscow KRISTALLOGRAFIYA in Russian  
Vol 36 No 3, May-Jun 91 pp 584-590

[Article by B. V. Merinov, A. I. Baranov, L. A. Shuvalov, and N. M. Shchagina, Institute of Crystallography, USSR Academy of Sciences]

UDC 548.736:537.723

[Abstract] An experimental study of new crystals with a high protonic conductivity,  $\text{Cs}_3\text{H}_3(\text{SeO}_4)_4 \cdot \text{H}_2\text{O}$  (CTSeM) was made for a determination of their atomic structure and phase transitions. Colorless transparent CTSeM single crystals for this study were grown by a static process from a supersaturated solution at room temperature. The phase transition temperatures were determined on the basis of differential thermal analysis in a 1500 Q derivatograph with a specimen heated at a rate of 5 K/min, also on the basis dielectric permittivity and electrical conductivity anomalies. Four anomalies were detected, one strong high-temperature anomaly at about 345 K and three weak ones at low temperatures. Optical and electrical measurements at temperatures covering the 100-380 K range were performed on 0.1 cm thick plates with 0.25-0.3 cm<sup>2</sup> surface areas with silver paste or vacuum-deposited silver layers as electrodes, each temperature having been stabilized within  $\pm 0.05$  K. Their electrical admittance at frequencies ranging from 30 kHz to 1 MHz was measured with an Ando Electric TR-10C bridge. For an X-ray structural and chemical analysis in Enraf Nonius CAD-4 precision automodiffractometer with a MoK $\alpha$ -radiation source and a graphite monochromator, single crystals were machined into spherical specimens 0.044 cm in diameter. Parameters of their rhombic primitive lattice (ferroelectric phase-II) were measured at room temperature and those of their hexagonal lattice (paraelastic phase-I) were measured at 360 K, the [100] orientation of phase-II coinciding with the [001] orientation of phase-I. The structural parameters were determined from the intensities of reflexes, taking into account the LP-factor and absorption of 158.4 cm<sup>-1</sup> radiation, and for calculation of the crystallographic parameters was used the AREN program package (V.I. Andrianov; KRISTALLOGRAFIYA Vol 32 p 228, 1987) was used for calculating the crystallographic parameters. The data indicate that three common eightfold d-positions in the rhombic phase are fully occupied by protons, these positions transforming into higher-multiple ones during transition to the hexagonal phase. Consequently, in the hexagonal phase the number of structurally equivalent position where protons can form hydrogen bonds will be larger than the number of protons available to occupy them. Figures 4; tables 2; references 17.

**Antiphase Interfaces in GaAs**

927J0038B Moscow KRISTALLOGRAFIYA in Russian  
Vol 36 No 3, May-Jun 91 pp 738-743

[Article by V. I. Vdovin, M. G. Milvidskiy, and T. G. Yugova, State Scientific Research and Design Institute of Rare Metals Industry]

UDC 548.4

[Abstract] An experimental study of antiphase interfaces in GaAs layers was made, defects of this kind forming and moving during epitaxial growth of layers of A<sup>III</sup>B<sup>V</sup> compounds. Such layers were grown by the MOS-hydride epitaxial method on Si(001) substrates with Si<sub>1-x</sub>Ge<sub>x</sub> transition layers and on Ge(001) substrates with either singular or vicinal surfaces. The transition layers on Si(001) substrates ( $x=1.2$ ,  $0.07 < \text{grad } x < 0.25$ ,  $x=1$ ) were grown by the method of gaseous chloride epitaxy, through a prior deposited 1-2  $\mu\text{m}$  thick Si surface layer. Examination of these GaAs/Si<sub>1-x</sub>Ge<sub>x</sub>/Si heterostructures was done under a Polivar-met microscope with a Nomarski contrast, under an SEM-515 scanning electron microscope in the induced-current mode, and under an IEM-200CX transmission electron microscope in the two-beam diffraction mode. Selective chemical etching which revealed antiphase interfaces was done with the DSL etchant and in a KOH melt. Under the scanning electron microscope were examined heterostructures with Schottky barriers which had been formed by vacuum deposition of a gold layer on the free GaAs surface. Examination under the transmission electron microscope was done in the plane of growth and in transversely cut sections. As a result of these examinations, antiphase interfaces were identified according to their geometrical pattern and their movement across the growing layer thickness was tracked on the same basis. The data indicate that antiphase interfaces and surface dislocations do not form together. As they come in contact, however, evidently anomalies of the stress distribution in the affected region cause these dislocations to become implanted in the antiphase interfaces. The latter thus inhibit propagation of glissile dislocations in the direction of epitaxial growth by actually pinning them. The geometrical pattern of antiphase interfaces may be related to the composition of the gaseous medium at the crystallization front. In this respect, therefore, epitaxially grown GaAs layers will be least defective when antiphase interfaces forming in the initial stage of the process are of one type and obliquely oriented so that they will annihilate each other as they intersect very near the GaAs/Ge or GaAs/Si<sub>1-x</sub>Ge<sub>x</sub> heterojunction. Figures 6; references 12.

**Characteristics of Defect Formation in Active Region of GaAlAs/GaAs Epitaxial Heterostructures for Solar Cells During Heating-Cooling Cycles**

927J0038C Moscow KRISTALLOGRAFIYA in Russian  
Vol 36 No 3, May-Jun 91 pp 750-756

[Article by A. A. Kalinin, M. G. Milvidskiy, T. A. Nuller, A. A. Shlenskiy, and T. G. Yugova, State Scientific Research and Design Institute of Rare Metals Industry]

UDC 548.4

[Abstract] An experimental study of GaAlAs/GaAs heterostructures used for solar cells was made concerning the formation of defects in their active region in the

process of their fabrication and subsequently during temperature cycles in service. Specimens of such an active solar cell region were produced by liquid-phase epitaxy on slices of GaAs single crystals as substrates with an A(111) orientation, these single crystals having been grown by the Czochralski method and doped with Sn to  $(3-5) \times 10^{17} \text{ cm}^{-3}$  concentrations. On such a substrate was epitaxially grown an 80  $\mu\text{m}$  thick GaAs layer with the same Sn-impurity concentration, this being done by programmed cooling of the GaAs melt from 850°C to 600°C. To serve as a wideband window, an about 10  $\mu\text{m}$  thick layer of  $\text{Ga}_{0.2}\text{Al}_{0.8}\text{As}$  solid solution was grown on top of the GaAs layer, also by liquid-phase epitaxy but in an independent process at a temperature of about 880°C. Metal contact tabs on this structure were deposited by the standard method. The thus built solar cells were then subjected to temperature cycles covering the -60°C to +60°C range. Defects forming during the fabrication process and then during these cycles were monitored by selective chemical etching in the A(111) plane of growth and sections cut obliquely at a 3° angle to the surface, also under a transmission electron microscope in the A(111) plane of growth and in transversely cut sections. The only defects found in a homogeneous epitaxial GaAs layer just grown on the substrate were dislocations as densely distributed as in as in that substrate. No other defects were found to have formed in this layer during subsequent stages of solar cell fabrication. Temperature cycling of complete solar cells was found to produce two types of defects in the epitaxial GaAs layer. One type of these defects were dense clusters of flat-bottom etch figures produced by "background corrosion" between dislocation pits. These defects in that layer were found to have formed only within its 20-30  $\mu\text{m}$  thick region under the GaAlAs top layer and within its region adjacent to the substrate underneath. The other type of defects were chains of small nondislocational etch figures forming "tracks" in the [110] directions. These defects were nonuniformly distributed over the thickness of a solar cell, most densely within its central region with the highest Ga concentration about 20-30  $\mu\text{m}$  above the GaAs substrate, none having formed at its boundary with the substrate underneath and at its boundary with the GaAlAs top layer. The structural transformations which produce defects in such solar are thus caused not only by formation and movement of dislocations during fabrication but evidently also by breakup of the solid solutions as these become supersaturated with one of the components during temperature cycling so that either excess As from the substrate or excess Ga in the epitaxial layer precipitates into dislocations. Figures 8; references 3.

#### Nanosecond Switching in Submicron-Size Sandwich Structures With Amorphous $\text{Ge}_x\text{Te}_{1-x}$ Film

927J0026A Vilnius LITOVSKIY FIZICHESKIY  
ZHURNAL in Russian Vol 31 No 3, May-Jun 91  
pp 318-325

[Article by E. Babenskas, S. Balevičius, A. Cenys, and N. Siktarov, Institute of Semiconductor Physics, LiSSR Academy of Sciences]

UDC 621.315.592

[Abstract] An experimental study of nanosecond switching in submicron-size amorphous thin-film  $\text{Ge}_x\text{Te}_{1-x}$  layers was made, a special sandwich structure having been designed and built for this purpose so as to avoid uncontrollable deformation and consequent uncertainty regarding size and shape of the active region created by a conventional clamp-on probe. The thickness of amorphous  $\text{Ge}_x\text{Te}_{1-x}$  films was varied from 0.03  $\mu\text{m}$  to 1.2  $\mu\text{m}$  and their composition varied over the  $x=0.15-0.25$  range. Such a film was deposited, by discrete vacuum evaporation, on the surface of a glass block surrounding a molybdenum probe. The probe was a molybdenum rod projecting from the center of a molybdenum plate exactly as high as the glass block. The rod had been tapered by electrochemical etching before it was inserted by fusion into this glass block from below till the glass block came to rest on the plate while the upper (smaller) face of the rod, flush with the surrounding glass surface, became a circular molybdenum "spot" under the Ge-Te film. The film was covered by a mesa structure consisting of 0.1  $\mu\text{m}$  thick Mo-layer underneath a 1  $\mu\text{m}$  thick Cr-Al electrode. The molybdenum plate carrying the glass block with this structure rested on an aluminum plate serving as the other electrode. Switching voltages were measured in a special test stand, with a fixed delay time, and switching current transients were recorded on an S7-19 oscillograph. On the basis of these measurements has been evaluated the dependence of both the electric field intensity in the active region  $E=V/d$  ( $V$ -switching voltage,  $d$ -interelectrode distance) and of the "short-circuiting" frequency not only on the interelectrode distance and thus on the thickness of the Ge-Te film but also on the composition of that film. The data indicate that nanosecond buildup of an electrical instability in such films is a multistage process, with the number of "steps" in the switching transient directly related to the film thickness. Evidently such a film placed between electrodes contains several discrete microswitches owing their existence to nonhomogeneity of the amorphous semiconductor material: regions of amorphous Te and  $\text{Ge}_x\text{Te}$  with crystalline GeTe inclusions. This hypothesis is consistent with the known structural characteristics of binary alloys such as these: two phases with different short-range orders and chemical compositions forming a granular structure with crystalline low-resistance inclusions while the amorphous regions form a random array of microswitches. A numerical simulation of the  $E=f(d)$  relation based on this hypothesis has yielded results which agree fairly well with the experimentally established relation. Figures 7; references 8.

#### Impact Ionization of Shallow Donors in n-InP Layers

927J0026B Vilnius LITOVSKIY FIZICHESKIY  
ZHURNAL in Russian Vol 31 No 3, May-Jun 91  
pp 326-332

[Article by A. Dargys, J. Kundrotas, J. Parseliūnas, and A. Cesna, Institute of Semiconductor Physics, LiSSR Academy of Sciences]

UDC 621.315.592

[Abstract] An experimental study was made concerning impact ionization of shallow donor impurities in weakly doped epitaxial n-InP layers, 4.5  $\mu\text{m}$  thick layers grown on insulating InP substrates. The mobility of donors and the excess of their concentration over acceptor concentration, measured at liquid-nitrogen temperature, were  $\mu \approx 10^5 \text{ cm}^2/(\text{V}\cdot\text{s})$  and  $n_D - n_A = 2 \times 10^{14} \text{ cm}^{-3}$  respectively. The degree of compensation in these layers was  $K = n_A/n_D = 0.63$ , with  $n_D + n_A = 9 \times 10^{14} \text{ cm}^{-3}$  according to Table 1 on page 4156 in PHYSICS REVIEW Vol 38B (1988) No 6. Contact tabs were formed on them by deposition of parallel NiGe, VaGe, and Au strips 4 mm apart and their subsequent burn-in at 470°C temperature in a hydrogen atmosphere. Across these contacts were applied nanosecond voltage pulses with a rise time of approximately 1 ns, whereupon the current passing through the layer over a period of 700 ns was monitored by measurements of the voltage drop across a 50  $\Omega$  series resistor. The amplitude of voltage pulses was varied so as to cover the 4.5-7.9 V/cm range of residual electric field intensity in the layers. With the current at its saturation level, their steady-state electrical conductivity was measured for a determination of its dependence on the electric field intensity over the 4.5-25 V/cm range and was found to begin approaching its saturation level  $\epsilon_{\infty} > 4 \Omega\cdot\text{cm}$  as the electric field intensity exceeded 15 V/cm. Analysis of the data and their theoretical interpretation are based on the following premises: 1) breakdown dynamics describable by a single discrete donor level in the conduction band, 2) electron transition from donors into the conduction band by impact ionization and their reverse transition into donors by thermal recombination, 3) electron mobility remaining constant and electron concentration as well as electric field intensity remaining uniformly distributed throughout the breakdown period, 4) characteristic time of electron energy relaxation much shorter than characteristic breakdown time. Ionization by the tunneling mechanism is disregarded, this effect being negligible in electric fields as weak as those under consideration. Both the ionization coefficient  $A_1 = [1 + (a_1/a_2)^{-1} K / (1-K)] / [1 + K / (1-K)]$  and the recombination coefficient  $B_1 = a_1 [(a_1/a_2)^{-1} - 1] / [1 + K / (1-K)]$  are calculated on the basis of this model, first the constant  $(a_1 = A_1 B_1 K / (1-K))$  being found with the aid of the  $n(t)/n_{\infty}$  curve representing the electron concentration (normalized to its steady-state level) as a function of time and passing through experimentally established points and then the constant  $a_2 = A_1 + B_1$  being found from the relation  $a_2 = a_1 (n_D - n_A) / n_{\infty}$ . Figures 4; references 10.

# **Effect of Electron Irradiation on Electric Properties and Photoluminescence of Nuclei-Doped Gallium Arsenide**

927J0047A Tomsk IZVESTIYA VYSSHIKH  
UCHEBNYKH ZAVEDENIY: FIZIKA in Russian  
Vol 34 No 4, Apr 91 pp 45-51

[Article by V. N. Brudnyy, D. L. Budnitskiy, N. G. Kolin, Ye. V. Malisova, M. P. Nikiforova, Siberian

Engineering Physics Institute imeni V. D. Kuznetsov at the Tomsk State University, a branch of the Physics-Chemistry Scientific Research Institute imeni L. Ya. Karpov]

UDC 621.315.592:537.312.5

[Abstract] Transmutation doping of complex semiconductors, including GaAs, for use in devices operating in high-energy radiation fields and the issue of radiation-stimulated changes in the properties of nuclei-doped GaAs (YaLAG) under electron irradiation are discussed. To this end, electric properties and photoluminescence (FL) of nuclei-doped GaAs crystals as well as conventional GaAs doped by the metallurgical method irradiated by electrons are investigated. Nuclei-doped GaAs n-type samples annealed after nuclei doping (YaL) were examined; the initial single crystals were grown by Czochralski's method, horizontal oriented crystallization (GNK), and gas phase epitaxy. The samples were irradiated with 1 MeV electrons at 300K and a fluence of  $1.1 \times 10^{15}$  to  $3.8 \times 10^{18} \text{ cm}^{-2}$ . The Hall effect, conductivity, and photoluminescence spectra were examined. The energy spectrum of radiation-induced defects (RD) is identical in nuclei-doped GaAs and conventional GaAs and adequately describes the dependence of the free electron concentration on fluence. Electron irradiation does not inject new radiative recombination centers compared to the initial state in both the nuclei-doped and conventional GaAs. Figures 5; tables 4; references 10: 9 Russian, 1 Western.

# **Effect of Electron Irradiation on Germanium-Doped Gallium Arsenide Properties**

927J0047B Tomsk IZVESTIYA VYSSHIKH  
UCHEBNYKH ZAVEDENIY: FIZIKA in Russian  
Vol 34 No 4, Apr 91 pp 82-86

[Article by V. N. Brudnyy, D. L. Budnitskiy, N. G. Kolin, Ye. V. Malisova, M. P. Nikiforova, Siberian Engineering Physics Institute imeni V. D. Kuznetsov at the Tomsk State University, a branch of the Physics-Chemistry Scientific Research Institute imeni L. Ya. Karpov]

UDC 621.315.592:537.312.5

[Abstract] The advantages of germanium added metallurgically into GaAs, especially its efficiency as a dopant with a low diffusivity and segregation, a low vapor pressure, and a high solubility in the liquid and solid phase and its amphoteric character which leads to an elevated degree of compensation and a low Hall charge carrier mobility are discussed. The irradiation dose and temperature dependence of the charge carrier concentration, mobility, and photoluminescence (FL) spectra and isochronous annealing of GaAs<Ge> and nuclei-doped GaAs (YaLAG) irradiated with electrons are investigated. To this end, GaAs<Ge> samples grown by Czochralski's method and nuclei-doped GaAs were

examined. The samples were irradiated at 300K with 1 MeV electrons at a fluence of  $1.1 \times 10^{15}$  to  $3.8 \times 10^{18} \text{ cm}^{-2}$ . The free electron concentration and mobility were determined by Hall effect and conductivity measurements within a 77-370K range. Photoluminescence spectra were recorded in a 0.9-1.55 eV range at 77K using a He-Ne laser. Isochronous annealing was conducted in a vacuum at a 100-800°C temperature. Data show that the energy spectrum of radiation-induced defects, radiative recombination centers, and basic reproduction stages of the electric and optical properties in GaAs<Ge> and nuclei-doped GaAs are similar, i.e., do not depend on the germanium doping method. Radiation-induced defects are less thermally stable in GaAs<Ge> than in nuclei-doped GaAs while the compensation degree related to the amphoteric impurity is lower in GaAs<Ge> than in nuclei-doped GaAs given an identical initial electron compensation. Figures 5; tables 1; references 8: 3 Russian, 5 Western.

#### Hall EMF in Compensated Semiconductors and Semimetals

927J0024A Leningrad FIZIKA TVERDOGO TELA  
in Russian Vol 33 No 4, Apr 91 pp 1150-1154

[Article by V. A. Kozlov and K. A. Sakharov, All-Union Scientific Research, Design Engineering, and Technological Institute of Current Sources]

UDC 621.362

[Abstract] A theory of the Hall effect in compensated semiconductors and semimetals is constructed for a narrow-bandgap one with an electron valley and a hole valley. The equation of kinetics for electrons and holes in a slab  $2d$  wide (from  $z = -d$  to  $z = +d$ ) and arbitrarily oriented relative to its crystallographic axes is  $v_e \delta \phi^{e,h} / dz \pm e(E_v) \pm e[v \times H] \delta f / \delta k = I^{e,h}$ , where the collision integral  $I^{e,h}$  also takes into account intervalley charge transfer and recombination. Inasmuch as the

scattering of charges is not elastic at low temperatures, this equation can be and is solved by the method of variation. The charge distribution in each valley is described by the function  $f = f(\epsilon - \xi) - \delta f / \delta w$  and an excess charge is then represented, in the diffusion approximation, by an additional term  $\phi(z, k) = \phi(z) + C_i(z) k_i$  on the right-hand side ( $\phi$  denoting the shift of chemical potential with the opposite sign). The variation principle and the inverse matrix yield a system of equations for the three parameters  $\phi^{e,h}$  and  $C_i$ , which are calculated here for a semiconductor or semimetal slab in a longitudinal magnetic field. Insertion of the thus obtained expressions for these parameters back into that system of equations yields a new system of two equations, namely for  $\phi^e$  and  $\phi^h$  in the two valleys, a new parameter  $L$  having been introduced which represents the diffusion length in the  $\tau$ -approximation and determines the charge distribution. This system of equations is solved under the condition of overall quasi-neutrality  $E_x(d) - E_x(-d) = 0$  and  $\int_{-d}^d (\phi^e - \phi^h) dz = 0$ . The solution reveals a strongly nonlinear potential profile across a slab, such a Hall effect having been discovered earlier in an experiment with bismuth slabs in a magnetic field (E.I. Rashba; ZHURNAL EKSPERIMENTALNOY I TEORETICHESKOY FIZIKI Vol 48, 1965). An expressions for the potential difference across such a slab is then readily obtained which indicates an essential role of diffusion and size effects, their contribution vanishing only when the diffusion lengths for electrons and holes are equal so that the  $(L_h^{-2} - L_e^{-2})$ -term is reduced to zero. When both diffusion lengths are  $L > d$ , which may be the case in ultrapure materials, then the transverse potential profile may become a cubic one. The opposite case of diffusion lengths  $L < d$  but  $L \gg \kappa^{-1}$  (Debye shielding length) is possible in a slab made "dirty" or in a magnetic field made sufficiently strong. When the diffusion lengths are  $L < \kappa^{-1}$ , then there is no space charge in the slab so that the Hall-effect electric field set up by surface charges becomes an almost uniform one. The authors thank V.S. Yegorov for experimental data and helpful discussions. References 5.

**Parametric Emission and Phase Conjugation of Intersecting Laser Beams in Nematic Liquid-Crystal Layer With Dye**

927J0027A Moscow PISMA V ZHURNAL  
EKSPERIMENTALNOY I TEORETICHESKOY  
FIZIKI in Russian Vol 53 No 12, 25 Jun 91 pp 586-590

[Article by O. L. Animonov and N. A. Dvoryaninov, Institute of Applied Physics, USSR Academy of Sciences, Nizhny Novgorod, V. Sheshkauskas, Vilnius University]

[Abstract] Parametric emission of intersecting radiation beams from a quasi-CW YAG:Nd<sup>3+</sup> laser and their phase conjugation during their simultaneous compatible Rayleigh scattering by a photorefractive thermal nonlinearity were observed for the first time, in a nematic liquid crystal containing a dye and approaching its transition to an isotropic liquid layer. In the experiment a continuous-wave YAG:Nd<sup>3+</sup>-laser with a lower than 2 W power rating emitted radiation in a single transverse mode with linear polarization. This radiation was modulated by a chopper into pulses with a repetition period 100 times longer than the pulse duration, the latter being varied over the 0.5-5 ms range. It was focused onto nonlinear layers of tolane and dye mixture forming nematic liquid crystals: a 0.5 mm thick layer and a 2 mm thick layer in cells between a transparent wall and a mirror wall, a 1 mm thick layer in a cell between two transparent walls. Onto the layer was also focused the radiation beam returning from the mirror wall (cells with 0.5 mm and 2 mm thick layers) or from of a semitransparent external mirror through the transparent wall (cell with 1 mm thick layer), this beam intersecting the pumping one at a small angle  $\theta_0$  off 180°. Planar orientation of the L=0.5 mm thick layer of nematic mixture with an absorption factor  $\alpha L \approx 0.4$  was effected by means of a surface orientator. Homeotropic orientation of the L=1 mm thick layer with an absorption factor  $\alpha L \approx 0.8$  and of the L=2 mm thick layer with an absorption factor  $\alpha L \approx 0.5$  was effected by means of an external alternating electric field applied across two conducting walls of the cell from a 50 Hz source with voltage regulation over the 30-500 V range. As the pumping power rose above a threshold level dependent on the geometry of both radiation beams and on the temperature of the nematic liquid crystal, an increasingly stronger backscattering of the radiation was observed in each cell. The temperature dependence of that threshold level and of the backscattering buildup time indicates a thermal nonlinearity mechanism involving temperature-dependent refractive indexes  $n_{o,e}$  for ordinary and extraordinary rays respectively, characterized by corresponding nonlinearity coefficients  $[dn]_{o,e}/\delta T$ . The space distribution of scattered radiation, recorded on I-1060 photographic film with the aid of an image converter, was found to depend on the angle between the intersecting radiation beams and on the focal length of the lens formed by constriction of the pumping laser beam in the nematic liquid crystal. This parametric character of scattered radiation emission by a nematic liquid crystal is substantiated theoretically on the example of two plane pump waves  $[E_0 \exp[i\omega_0 t + ik''r]]$  intersecting in a medium with a

thermal nonlinearity. When the thermal lattice builds up faster than it becomes blurred as a consequence of thermal conductivity, its buildup is exponential in time and scattering waves are generated. This occurs in a mode which depends on the frequency mismatch between the two waves as the determining parameter. When the counter-propagating wave originates from a mirror boundary of the layer with thermal nonlinearity, then the frequency mismatch necessary for a minimum emission threshold depends on the reflection coefficient of that mirror boundary and on the radiation absorption by that nonlinear medium. When the nonlinear layer is pumped by two opposing speckle-beams, then the process becomes analogous to phase conjugation during stimulated scattering. Another factor likely to influence the space distribution of scattered radiation emission by a nematic liquid crystal would be an increase of the coefficients  $\delta_{o,e}T$  characterizing the thermal nonlinearity. The authors thank V.I. Bespalov, P. Adomenas, and G.A. Pasmanik for support and helpful discussions. Figures 2; references 6.

**Photoelectron Emission by Surfaces of Materials Exposed to Short-Wave Radiation**

927J0023A Leningrad PISMA V ZHURNAL  
TEKHNICHESKOY FIZIKI in Russian  
Vol 17 No 12, 26 Jun 91 pp 5-8

[Article by O. B. Ananin, Yu. A. Bykovskiy, A. A. Zhuravlev, and V. Yu. Znamenskiy]

[Abstract] An experimental study of photoelectron emission by a surfaces of various materials exposed to short-wave radiation was made, a copper plasma generated a Nd-laser beam serving as the source of such a radiation. The plane surface of a copper target was treated with that laser beam in pulses of 12 J energy and 10 ns duration. A concentrator lens then collected the radiation coming from that plasma within a solid angle of about 0.02 sr and focused it onto a spot about 3 mm in diameter at a distance of 0.5 m from the photoelectron emitter surface, thus ensuring a high radiation intensity up to about 0.5 MW/cm<sup>2</sup> and elimination of otherwise incident particles at that surface. The form of the radiation spectrum at the exit from the concentrator lens was rather intricate, with maximum intensity within the 5-7 nm band. As photoelectron emitter materials were tested C, Be, Cu, Ti, Si, (CH<sub>2</sub>)<sub>m</sub>, K8 quartz glass, acrylic glass, and teflon (polytetrafluoroethylene). Photoelectron emission currents were recorded by the standard collector method in the saturation mode under a pressure of about 1 m torr. The quantum yield from these emitters, estimated on the basis of the data, was found to vary within the 0.04-0.4 percent range. The copper photoelectron emitter was also tested under exposure to radiation within the 0.8-2.0 nm band, this radiation having passed through a filter consisting of a 1  $\mu$ m thick dacron (polyethylene terephthalate) layer and a 0.2  $\mu$ m thick aluminum layer. The results indicate that decreasing the wavelength of

incident radiation increases the quantum yield of photoelectron emission by most materials. Figures 2; tables 1; references 4.

#### Auger-Transition 108.9 nm Xe-Laser Pumped by "Atomic" Bremsstrahlung From Proton Beam

927J0023B Leningrad PISMA V ZHURNAL  
TEKHNICHESKOY FIZIKI in Russian Vol 17 No 12,  
26 Jun 91 pp 47-50

[Article by A. D. Andreyev and V. V. Ryzhov, Institute of High-Current Electronics, Siberian Department, USSR Academy of Sciences, Tomsk]

[Abstract] The emission characteristics of an Auger-transition Xe-laser pumped with "atomic" bremsstrahlung have been calculated, experiments having been performed by several researchers which involved ionization of the 4d-subshell of a neutral Xe atom by soft x-rays and subsequent ionization of the Xe-II ion into a Xe-III ion by way of a fast Auger-decay with attendant population inversion between the  $5s^05p^6-4s^0$  and  $5s^15p^5P_1$  levels. Tantalum plasma was used as the source of soft X-rays, such a plasma being generated by focusing a Nd-laser beam onto a tantalum target, radiation emitted by this plasma then exciting the Xe-laser into emission of 108.9 nm radiation with an efficiency up to 0.01 percent and a gain  $\alpha$  up to  $2.3 \text{ cm}^{-1}$  depending on the Nd-laser power. Pumping a xenon atom with "atomic" bremsstrahlung emitted by a charged high-energy particle such as a proton or ion on that atom is considered as an alternate method, inasmuch as both the maximum intensity of such a bremsstrahlung and the maximum cross-section for photoionization of the 4d-subshell lie within the spectral range which corresponds to the range of 4d-subshell ionization potentials. A set of programs written for simulation and numerical analysis of the entire process beginning with injection of energy into the gaseous active medium and ending with extraction of radiation from it, was used for the calculations. These included solution of a system of differential equations describing the kinetics of laser levels (M.Ya. Amusya, V.M. Buymistrov, B.A. Zon, et al.; "Polarized Bremsstrahlung Emission by Particles and Atoms", Izd. Nauka, Moscow 1987), using experimentally determined values of the constants (G.-Y. Yin, C.P. Barty, D.A. King, D.J. Walker, and S.E. Harris: OPTICS LETTERS Vol 12 No 5, 1987). There was thus evaluated the dependence of the gain  $\alpha$  and of the power  $Q$  of spontaneous emission at the 108.9 nm wavelength on the xenon pressure  $P$ , at a fixed  $j = 15 \text{ kA/cm}^2$  current density of the pumping proton beam. Both the gain  $\alpha$  and the power  $Q$  of spontaneous emission at the same wavelength were also calculated as functions of time over a period of 100 ns, the duration of such a proton current pulse, for xenon under a pressure of 35 torr. The results indicate that the maximum gain in this scheme would be  $\alpha \approx 0.04 \text{ cm}^{-1}$  and the coefficient of conversion of proton beam energy into radiation quanta (108.9 nm wavelength) energy would be of the

order of  $10^{-7}$ . The main advantage of proton beam pumping is the possibility of exciting large volumes of gas and exciting them into superemission. Figures 2; references 8.

#### Threshold Characteristics of Laser With Nuclear Pumping of Transitions in Xe-Atom

927J0023C Leningrad PISMA V ZHURNAL  
TEKHNICHESKOY FIZIKI in Russian Vol 17 No 12,  
26 Jun 91 pp 78-82

[Article by S. P. Melnikov and A. A. Sinyanskiy]

[Abstract] Pumping of He-Xe and Ar-Xe lasers with nuclear radiation is considered, with thermal neutrons produced by uranium fission as the radiation source. The feasibility of such a scheme having already been established in experiments with He-Xe, Ar-Xe, and He-Ar-Xe mixtures containing up to about 1 percent Xe, the effectiveness of this scheme is evaluated theoretically in terms of the threshold neutron flux density and its dependence on both pressure and composition of the gas. Calculations were made on the basis of the authors' kinetic model (A.M. Voinov, S.P. Melnikov, and A.A. Sinyanskiy; ZHURNAL TEKHNICHESKOY FIZIKI Vol 60 No 10, 1990; IZVESTIYA AKADEMII NAUK SSSR: SERIYA FIZICHESKAYA Vol 54 No 10, 1990) describing the fundamental plasma processes of energy transfer from the buffer gas to the upper  $5d(3/2)_1^0$  level in a xenon atom and the quenching of this level by collisions with He, Ar, Xe atoms in the ground state. This level was assumed to become populated selectively and almost 100 percent efficiently, owing to dissociative recombination of molecular  $\text{Xe}_2^+$  ions with electrons. Nine reactions were accounted for in a He-Xe mixture and twelve reactions were accounted for in a Ar-Xe mixture. The input data matched the conditions of the authors' experiment: 200 cm long active region, pump pulse of about 4 ms duration with a maximum corresponding to  $1.1 \times 10^{15} \text{ cm}^{-2} \text{ s}^{-1}$  mean over-the-region number of thermal neutrons. The threshold neutron flux density and also the unsaturated gain at the maximum of the pump pulse were calculated on this basis, assuming no losses in the optical cavity. The calculations for a He:Xe = 1000:1 mixture lasing at the  $2.65 \text{ }\mu\text{m}$  wavelength have yielded the dependence of both parameters on the total pressure of this mixture up to 6 atm. The calculations for Ar-Xe mixtures lasing at the  $1.73 \text{ }\mu\text{m}$  wavelength have yielded the dependence of these two parameters on the partial xenon pressure over the 0.1-20 mm Hg range at a fixed argon pressure of 0.5 atm and on the argon pressure up to 1.5 atm at a fixed partial xenon pressure of 2 mm Hg. The results of these calculations agree fairly well with experimental data, except for an underestimation of the actual threshold neutron flux density at higher argon pressures under which losses in the optical cavity become appreciable. Figures 2; references 11.

# Amplitude and Frequency Characteristics of Double-Mode Ring Lasers With Controllable Phase Anisotropy

927J0019A Moscow KVANTOVAYA ELEKTRONIKA  
in Russian Vol 18 No 6, Jun 91 pp 681-684

[Article by V. I. Timofeyev]

UDC 621.378.3

[Abstract] Interaction of electromagnetic waves in a ring cavity with controllable phase anisotropy of a double-mode (s,n) gas laser in an arbitrarily orient magnetic field is considered, such lasers being of interest as instruments for simultaneous measurement of several physical quantities on the basis of beat frequencies which characterize interaction of two waves s,n propagating in one direction and two waves s',n' propagating in the opposite direction. The theoretical analysis of their interaction is based on a system of three nonlinear differential equations for the rates of change of slowly varying amplitudes  $A_s, A_n$  of two unidirectional waves and the rate of change of their phase difference  $\varphi_{sn}$ . This system of equations has been derived by E.G. Pestov's method for two counterpropagating waves (KVANTOVAYA ELEKTRONIKA Vol 11 p 1592, 1984), but it contains additional terms proportional to the combination interaction coefficients  $\eta_{snn}$  and  $\rho_{snn}$ . A solution of these equation by approximation methods yields expressions for the sum and the difference of their intensities (amplitudes squared), which indicate that the amplitude characteristics of waves in a double-mode ring laser with a smoothly adjustable mode separation are determined above all by the interaction coefficients  $\tau, \kappa, \eta, \rho$ . From the third equation of that system is derived a differential equation for half the sum of their phases  $\varphi_{sn}^{(m)} = (\varphi_{sn} + \varphi_{s'n'})/2$ . This equation is solved, considering that  $d\varphi_{sn}^{(m)}/dt \ll d\varphi_{sn}/dt$  and by therefore averaging the intermode beat frequency over a multiple of the period corresponding to the difference frequency. For two unidirectional waves and two counterpropagating waves in an open optical cavity is then obtained the dependence of their respective intermode beat frequencies on their respective frequency differences and on the laser characteristics, particularly on the difference between dissipation and amplification of different waves by the active medium. The results reveal additional frequency shifts which degrade the accuracy of measurements, principally due to asymmetry of the active medium and ring cavity characteristics with respect to unidirectional waves and with respect to counterpropagating ones. The beat frequency of counterpropagating waves is found to be further shifted by combination interaction and amplitude modulation of unidirectional ones. Minimizing the frequency shifts of intermode beats of unidirectional waves thus requires not only attenuation of counterpropagating waves but also equal tuning of the cavity modes relative to the center of the Doppler contour, placement of the active medium in a longitudinal magnetic field, and linear or identical other

polarization of the electromagnetic waves. A typical application for such a ring laser, with a photoelastic element inside the optical cavity, is simultaneous measurement of angular velocity and linear acceleration of a target. The author thanks E.G. Pestov (deceased) and G.S. Kruglik for helpful discussions. References 11.

# Dynamics of Spectral and Angular Excimer-Laser Radiation Emission Characteristics

927J0019B Moscow KVANTOVAYA ELEKTRONIKA  
in Russian Vol 18 No 6, Jun 91 pp 684-688

[Article by A. G. Zhidkov, A. O. Tersikh, and S. I. Yakovlenko, Institute of General Physics, USSR Academy of Sciences, Moscow]

UDC 621.373.826.038.838

[Abstract] The radiation emission characteristics of excimer power lasers are analyzed theoretically, taking into account the appreciable parasitic amplification of spontaneously emitted radiation and the frequency dependence of amplified radiation as well as the narrowing of the  $2 \rightarrow 1$  lasing resonance transition line in the amplifying medium. The analysis is based on the three-dimensional equation of radiation transfer and on a modification of the "particle-in-cell" method for the open two-level model. Disregarding wave interactions, the evolution of radiation (frequency  $\omega$ ) emission in space and time is accordingly described by both the rate of change and the gradient of its intensity  $I(\omega, n, r)$  at some point  $P(r, n)$  ( $r$ -radius vector in the direction of unit vector  $n$ ):  $\delta I(\omega, n, r)/\delta t + n \delta I(\omega, n, r)/\delta r = [\kappa^*(\omega, r, t) - \kappa^-(\omega, r, t)] I(\omega, n, r) + Q(\omega, n, r, t)/4\pi$  ( $t$ -time,  $c$ -speed of light,  $\kappa^+$ - gain at  $2 \rightarrow 1$  lasing transition,  $\kappa^-$ - coefficient of nonresonant absorption of useful radiation,  $Q$ - power of spontaneous radiation emission). The populations of the two levels are described by a system of two coupled equations for their respective rates of change. A comparative evaluation of the dynamics of radiation emission by an excimer laser inside an optical cavity between two plane mirrors and inside a telescopic cavity is made, two such lasers having been tested: 1) 308 nm XeCl-laser (Ne:Xe:HCl=2500:100:6 gas mixture under total pressure of 3.2 atm uniformly pumped by an electron beam), 2) 248 nm KrF-laser (Ar-Kr-F<sub>2</sub> mixture under a total pressure 1.75 atm pumped with an energy of 50 kW/cm<sup>2</sup>). The radiation emission characteristics of each have been calculated as functions of time covering the transient period of 20-30 ns into the subsequent steady state, these characteristics being the radiation pattern as indicator of the beam divergence, the radiation intensity along the axis of the optical cavity, and the spectral width of the  $2 \rightarrow 1$  transition line. The dependence of that line width on the optical thickness of the active medium in the absence of saturation was obtained from the solution to the one-dimensional equation of radiation transfer (intensity a function of frequency only), both on the basis of the integral radiation emission intensity and in the

effective line width  $\Delta\omega = 1/S(\omega_0)$  approximation ( $L$  - length of active medium). A quantitative analysis of the results reveals that calculations based on the effective line width yield a fairly accurate estimate of the beam divergence but underestimate the absolute radiation intensity, the difference being negligible when the amplification saturation range is considered and becoming appreciable when the high-gain range  $\kappa^*L > 1$  below saturation of the active medium is considered. A numerical evaluation of that relation for a two-pass KrF-laser inside an optical cavity between two ideal plane mirrors with reflection coefficients  $R_1 = 0$  and  $R_2 = 1$  respectively confirms those conclusions. Figures 12; references 17.

### Radiation Emission Characteristics of Pulsed CO<sub>2</sub>-Laser in Unstable Optical Cavity With Nonuniform-Reflectance Exit Mirror

927J0019C Moscow KVANTOVAYA ELEKTRONIKA  
in Russian Vol 18 No 6, Jun 91 pp 697-698

[Article by M. N. Kuznetsov and O. L. Kulikov, Institute of Problems in Mechanics, USSR Academy of Sciences, Moscow]

UDC 621.373.826.038.823

[Abstract] An experimental study of a pulsed CO<sub>2</sub>-laser in an unstable optical cavity with a semitransparent "soft" exit mirror was made, the reflection coefficient smoothly decreasing from the center toward the periphery of this mirror and thus along the radius of the incident radiation beam. The active medium of the laser was a CO<sub>2</sub>:N<sub>2</sub>=1:1 gas mixture occupying a 40x60x700 mm<sup>3</sup> large volume under a pressure of 0.25 atm for transverse excitation by electric discharge. The optical cavity, set for an  $M=1.47$  magnification, was formed by a convex spherical mirror with a 40 m radius of curvature and a plane semitransparent exit mirror behind a  $D=35$  mm diameter diaphragm. The object of the first experiment was to compare the radiation emission characteristics attainable by use of such a "soft" exit mirror with those attainable by use of a regular exit mirror with a sharply defined periphery and by use of an exit mirror with a smoothed periphery, the cavity configuration remaining otherwise unchanged and the active medium being identically excited by pulses pumping 150 J/dm<sup>3</sup> energy into it. The regular mirror was a bilaterally cleared plate with a semitransparent ZnSe-coating deposited on one side through a hole in a mask so that it formed a circular aperture for the radiation beam, the mask having been placed before the plate at a close distance. The mirror with a smoothed periphery was a bilaterally cleared ZnSe-plate with a semitransparent coating apodized so as to prevent a phase shift in the passing radiation beam and with a reflective ZnSe-BaF<sub>2</sub>-ZnSe-BaF<sub>2</sub> multilayer coating (ZnSe- large refractive index, BaF<sub>2</sub>- small refractive index) deposited on one side through a hole in a mask so that it formed a circular aperture for the radiation beam, the mask having been placed before the plate at a distance which

would ensure formation of an approximately  $r/2N_F \approx 3$  mm wide smooth peripheral zone ( $r$ - radius of exit mirror,  $N_F$ - equivalent Fresnel number). The "soft" mirror was a similar plate bilaterally cleared with multilayer BaF<sub>2</sub>-ZnSe-BaF<sub>2</sub>- ZnSe coatings (1.1  $\mu$ m thick BaF<sub>2</sub>, 0.21  $\mu$ m thick ZnSe) and then coated on one side with a ZnSe film whose thickness tapered smoothly from a quarter wavelength at the center to a smaller one at the periphery, this film having been deposited through a mask rotating simultaneously about its own axis and about the axis of its 80 mm diameter frame. Measurements were first made with a small diaphragm moving from the center of the mirror to its periphery, the "soft" exit mirror having been found to produce the smoothest radiation intensity distribution within the near-field zone. Measurements were then made with a semitransparent beam-splitter plate which diverted one part of the laser radiation to a calorimeter for monitoring the energy of emission pulses and sent the other part to a concave spherical mirror mounted 4.5 m away in the far-field zone. This mirror, with a 60 mm base diameter and a 20 m radius of curvature, reflected that part of the laser radiation through an iris diaphragm into another calorimeter for monitoring the laser beam divergence. That divergence was found to have been minimized by use of the "soft" exit mirror. In the second experiment the energy of the fraction of laser radiation propagating within a conical sector with a vertex angle  $\theta = 2.44\lambda/D$  ( $D$ - diameter of aperture stop,  $\lambda$ - radiation wavelength) equal to the diffraction angle was measured as the excitation energy was being varied over a wide range. With the "soft" exit mirror, unlike with the regular one, the fraction of laser radiation energy within that sector did not change appreciably and remained close to the diffraction limit over the entire 50-200 J/dm<sup>3</sup> range of excitation energy. The authors thank V.V. Ragulskiy for discussing the results and M.I. Baklushina for preparation of the interference coatings. Figures 2; tables 1; references 10.

### Flow Patterns Resulting From Interaction of Twin CO<sub>2</sub>-Laser Pulses and Target in Air

927J0019D Moscow KVANTOVAYA ELEKTRONIKA  
in Russian Vol 18 No 6, Jun 91 pp 704-707

[Article by A. A. Bakeyev, L. I. Nikolashina, M. N. Potashkin, and N. V. Prokopenko, Scientific-Industrial Association "Astrofizika", Moscow]

UDC 621.373.826:533.9

[Abstract] Action of two successive twin CO<sub>2</sub>-laser pulses on a solid target in air and the resulting gas dynamic flow patterns above such a target are analyzed theoretically with the aid of available experimental data, experiments having been performed with a duralumin target in standard air and two successive identical pulses of coherent 10.6  $\mu$ m radiation from a high-pressure CO<sub>2</sub>-laser. This laser was preionized by corona discharge and excited by electric discharge pulses, two separately

energized discharge banks having been placed inside the common optical cavity so that the two successive emission pulses could be generated independently with any time interval between them. The total duration of each pulse was 2.7-3  $\mu$ s, including a not wider than 0.2  $\mu$ s wide peak within which the intensity reached a level 4-6 times higher than the maximum intensity during the remainder and which contained 15-20 percent of the total pulse energy. The time interval between pulses was varied over the  $\Delta t = 3-12 \mu$ s range. The first pulse generated a "hot gas" plasma, which then spread out during the post-pulse period until, as a result of adiabatic and radiative cooling, its pressure became equal to the pressure of the ambient "cold air". The gas dynamic flow pattern developing by action of the second pulse depended largely on the time interval between the two. Plasma expansion was recorded by SFR-2M streak cameras. The data are first interpreted hypothetically in terms of two waves: 1) a shock wave traveling toward the target and impinging on it, 2) an "outward" wave leaving the target and then absorbing the entire laser radiation while traveling against the laser beam. A shock wave could have been formed in two ways, either following absorption of the pulse peak energy within a small gas volume or by piston action of the hot gas within the absorption wave. The first mechanism is not consistent with estimates based on the theory of plane shock, according to which the energy required for formation of such a shock wave would be about the total pulse energy. The second mechanism would be plausible only to the extent that the absorption wave leaving the target slowed down after some time, but this did not happen upon impact with a shock wave reflected by the target immediately after optical breakdown at the hot gas and cold gas interface. Estimates based on the theory of fast processes do not agree with those based on experimental data. Most likely, according to calculations based on equations of gas dynamics for an ideal gas, not a shock wave but an "overcompressed" detonation wave with an absorption front pushed by a gaseous "piston" traveled toward and impinged on the target. The authors thank R. Ye. Rovinskiy and N.N. Vorobyeva for assisting in the experiments, and A.P. Sobolev for helpful discussion of the results. Figures 2; tables 2; references 11.

#### Feasibility of Picosecond Terawatt Nd-Laser With About $10^{13}:1$ Contrast Ratio

927J0020A Moscow KVANTOVAYA ELEKTRONIKA  
in Russian Vol 18 No 5, May 91 pp 534-535

[Article by L. L. Losev, A. P. Lutsenko, and S. N. Sazonov, Institute of Physics imeni P. N. Lebedev, USSR Academy of Sciences, Moscow]

UDC 621.373.826.038.825.3

[Abstract] A scheme of a neodymium glass laser is proposed which will emit 1.056  $\mu$ m radiation in terawatt pulses of picosecond duration with a pulse rise time of the order of 1 ps and with an intensity contrast ratio of

the order of  $10^{13}:1$ . The optical system of this laser includes a mode-locked master ruby laser-oscillator which generates trains of pulses of about 30 ps duration, an electrooptical shutter which extracts from such a train a single pulse, a ruby laser-amplifier which boosts the energy of this pulse to 3-5 mJ, a dichroic mirror, and a Raman cell filled with gaseous  $SF_6$  under a pressure variable from 5 to 20 atm for stimulated backscattering of the incident radiation. The amplified pulse is so focused onto the Raman cell that it will be maximally compressed during stimulated scattering and generation of a 0.734  $\mu$ m Stokes radiation component (Stokes shift 775  $cm^{-1}$ ). The maximum attainable pulse compression has been calculated in the one-dimensional approximation with the aid of available experimental data, taking into account nonsteadiness of molecular vibrations and of the focusing process. The dichroic mirror between the laser-amplifier and the Raman cell is oriented at a 45° angle to the optical axis and passes the amplified laser pulse to the Raman cell. It also extracts a backscattered Stokes pulse of 1-2 mJ energy and about 1 ps duration by reflecting it into another cell, one filled with hydrogen under a pressure variable from 15 to 150 atm, where stimulated scattering at vibrational levels of hydrogen molecules (Stokes shift 4155  $cm^{-1}$ ) builds up while this pulse is being focused. This cell is followed by an IKS-7 infrared glass filter which extracts the first Stokes component, the frequency of this 1.0556  $\mu$ m component coinciding with the center frequency of the amplification line of GLS21 and GLS22 (phosphate glass):Nd lasers within  $\pm 10 cm^{-1}$ . The extracted first Stokes component passes through three amplifier stages to a harmonic generator consisting of two KDP crystals one behind the other, the fourth-harmonic radiation pulses then being focused by an F/3 lens onto the target. The contrast ratio attainable in this laser system is limited by the finite Contrast ratio in the shutter and by noise in the amplifiers. With an about 100:1 standard contrast ratio in the electrooptical shutter, the intensity of emitted subpulses will be determined by luminescence of the amplifiers and should not be higher than the intensity of the useful pulse divided by  $10^{20}$  Figures 2; references 7.

#### New Laser Crystal Emitting Dark-Red Radiation at 300 K Temperature

927J0020B Moscow KVANTOVAYA ELEKTRONIKA  
in Russian Vol 18 No 5, May 91 pp 535-536

[Article by A. A. Kaminskiy, Institute of Crystallography imeni A. A. Shubnikov, USSR Academy of Sciences, Moscow, and A. G. Petrosyan, Institute of Physics Research, ArSSR Academy of Sciences, Ashtarak]

UDC 621.373.826.938.825.2

[Abstract] A new laser has been produced, namely a  $LuAlO_3:Pr^{3+}$  single crystal emitting dark-red radiation at 300 K temperature. Sufficiently large single crystals of high optical quality were successfully grown despite the instability of the  $LuAlO_3$  compound below its solidus

line and low thermal stability at temperatures above 1000°C. Having discovered that crystallization centers of the metastable  $\text{LuAlO}_3$  phase are retained during transition to the crystallization equilibrium temperature, the authors pulled such crystals by the Bridgman method in molybdenum containers. They were grown from a melt of LuO-D-grade  $\text{Lu}_2\text{O}_3$  and vacuum-fused leukosapphire containing 0.75 atom.percent  $\text{Pr}^{3+}$  ions, the containers being pulled down at a rate of about 1.5 mm/h. In rhombic  $\text{LuAlO}_3$  crystals with an ordered structure of the  $D_{2h}^{16}$ -P6mm space group the  $\text{Pr}^{3+}$  ions replaced  $\text{Lu}^{3+}$  ions in the C<sub>2</sub> positions (coordination number 12). Laser specimens were cut from the crystals in the form of 50 mm long rods 5 mm in diameter with plane-parallel (within 5") bases. These specimens were placed inside an ellipsoidal luminaire with a silver-coated active surface and excited by an ISP-250 xenon flash lamp with long-wave radiation beyond the 0.425  $\mu\text{m}$  edge in pulses of approximately 25  $\mu\text{s}$  duration. Various spherical mirrors with an  $r \approx 500$  mm base radius and multilayer dielectric mirrors with a  $T \approx 0.005$  transmission coefficient for the laser radiation were used for forming a confocal optical cavity. Emission was stimulated at two transitions:  $^3\text{P}_0 \rightarrow ^3\text{F}_3$  (excitation threshold energy 12 J, energy of final laser level approximately 6520  $\text{cm}^{-1}$ , width of luminescence line approximately 4.5  $\text{cm}^{-1}$ ) and  $^3\text{P}_0 \rightarrow ^3\text{F}_4$  (excitation threshold energy 10 J, energy of final laser level approximately 7030  $\text{cm}^{-1}$ , width of luminescence line approximately 15  $\text{cm}^{-1}$ ), both transitions falling within the dark-red region of the radiation spectrum. The authors thank A.A. Markosyan and K.L. Ovanesyan for assistance in preparation and study of the crystals. References 5.

#### Pulsed Laser ISKRA-5 With 120 TW Power Rating

927J0020C Moscow KVANTOVAYA ELEKTRONIKA in Russian Vol 18 No 5, May 91 pp 536-537

[Article by V. I. Annenkov, V. A. Bagretsov, V. G. Bezuglov, L. M. Vinogradskiy, V. A. Gaydash, I. V. Galakhov, A. S. Gasheyev, I. P. Guзов, V. I. Zadorozhnyy, V. A. Yeroshenko, A. Yu. Ilin, V. A. Kargin, G. A. Kirillov, G. G. Kochemasov, V. A. Krotov, Yu. P. Kuzmichev, S. G. Lapin, L. V. Lvov, M. R. Mochalov, V. M. Murugov, V. A. Osin, V. I. Pankratov, I. N. Pegoyev, V. T. Punin, A. V. Ryadov, A. V. Senik, S. K. Sobolev, N. M. Khudikov, V. A. Khrustalev, V. S. Chebotar, N. A. Cherkesov, and V. I. Shemyakin, All-Union Scientific Research Institute of Experimental Physics, Arzamas (Nizhnegorodsk Oblast)]

UDC 621.373.826.038.823

[Abstract] A pulsed iodine laser has been built at the Institute for experiments with laser-induced thermonuclear fusion, stimulated radiation emission and amplification in such lasers occurring upon photodissociation of alkyl iodide molecules with attendant preferential generation of excited iodine atoms  $\text{I}(^2\text{P}_{1/2})$  and the emitted

radiation corresponding to the  $^2\text{P}_{1/2} \rightarrow ^2\text{P}_{3/2}$  transition. This laser "Iskra-5" includes an actively mode-locked master oscillator and 12 amplifier stages. The oscillator generates radiation pulses of about 1 mJ energy and about 0.5 ns duration, their energy being boosted to 8 J by passage through the preamplifier stages. The laser beam is split into 12 equal ones in terms of energy content, their energy being boosted in 5 amplifier stages with an incremental aperture each. The first two stages are pumped by xenon flash lamps uniformly spaced around the active medium in a quartz cell and in turn surrounded by reflectors. The third stage is pumped by a xenon flash lamp held directly in the active medium. The two end stages are pumped by repetitive electric discharges. Spatial filters and decoupling cells with dye solution placed between the amplifier stages prevent self-excitation of the amplifiers and improve optimize the beam geometry. In a full-scale experiment was obtained a laser beam with a divergence of only approximately 0.1 mrad carrying pulses of 30 kJ energy and 0.25 ns duration. The building specially designed for this "Iskra-5" laser has four floors, enough for accomodating all the 12 amplifier stages. Figures 3; references 9.

#### Electric-Discharge Excimer XeCl-Laser Generating Long Emission Pulse

927J0020D Moscow KVANTOVAYA ELEKTRONIKA in Russian Vol 18 No 5, May 91 pp 560-562

[Article by V. V. Atezhev, V. S. Bukreyev, S. K. Vartapetov, I. A. Veselovskiy, A. N. Zhukov, I. T. Ziganshin, A. Z. Obidin, and A. Ye. Soldatkin, Institute of General Physics, USSR Academy of Sciences, Moscow]

UDC 621.373.826.038.823

[Abstract] An experimental study has established the feasibility of converting the "Model 1701" pulsed electric-discharge excimer XeCl-laser into a commercially producible one emitting single-frequency radiation pulses of long duration. For this the discharge system was modified by addition of an independent array of preionizing spark gaps, one row of them on each side of the main discharge in the plane of the anode inside the hermetically closed discharge chamber, and by using two TGI-1-1000/25 thyatrons as switches. The main electrodes were spaced 2.2 cm apart and the active medium, a Ne-Xe-HCl gas mixture, occupied 2.2x1x50  $\text{cm}^3$  of the interelectrode space. The optical cavity was formed by two plane mirrors, with an  $R=0.35$  reflection coefficient at the exit mirror. Both energy and duration of an emission pulse were found to increase as the capacitance in the preionization circuit was increased up to 6.6 nF, neither of them increasing further with a still larger capacitor in that circuit. Neither of them was found to change appreciably as the time interval between firing of thyatron 1 to firing of thyatron 2 was varied over the 50-600 ns range. With a 6.6 nF preionization capacitor, a 60 nF storing capacitor, and two 2 nF peaking capacitors, a pulse of 140 mJ maximum energy and 180 ns

duration (at half-amplitude level) was obtained by using a Ne:Xe:HCl= 400,000:2600:260 gas mixture under a total pressure of  $4 \times 10^5$  Pa and a pulse of only 30 mJ energy but 250 ns maximum duration (at half-amplitude level) was obtained by using a Ne:Xe:HCl= 200,000:130:55 gas mixture under a partial Ne pressure of 4 atm. The pulse duration decreased almost linearly with decreasing Xe and HCl concentrations, but at constant Xe and HCl concentrations did not decrease while the pulse energy increased with increasing partial Ne pressure. Further experiments were performed with transmission of such long laser pulses through optical fibers. For this the plane opaque mirror was replaced with a corner reflector and the plane exit mirror was replaced with two half plates, one opaque with an R= 1 reflection coefficients and with an R= 0.35 reflection coefficient so aperture for the laser beam was reduced to one half. The laser beam was thus narrowed to a 1 cm square cross-section, with almost no loss of energy. So extracted, it was passed through a diaphragm (10 mm diameter) and then a lens (40 mm focal length) which projected the diaphragm onto the entrance aperture of a quartz fiber with a 520  $\mu$ m in diameter core. Pulses of 40 mJ energy and 150 ns duration were recorded leaving the fiber at the other end. Compression of the emission spectrum was achieved by placing the laser inside a 1.2 m long dispersive optical cavity between an opaque plane mirror and a diffraction grating with 2400 lines/mm, in an arrangement which ensured autocollimation. For spatial selection of transverse modes, a circular 1.5 mm in diameter diaphragm was placed on each side of the discharge chamber. Further compression of the spectrum to a width  $\Delta\lambda < 0.1$  nm was effected by placing two Fabry-Perot etalons with a sharpness index of 12 inside the optical cavity, an "air" etalon with a 3 mm wide base and a solid-state etalon with a 28 mm wide base, at small angles to the optical axis. The width of the spectrum was monitored with an interferometer (3 mm wide base, 0.01  $\text{cm}^{-1}$  wide passband). Simultaneous measurements made with a high-speed photodiode followed by an amplifier revealed no intermode beats along the pulse envelope, indicating a near single-frequency emission. Figures 4; references 6.

# **New Class of Solitons in Optical Fibers Near Zero-Dispersion Point**

927J0020E Moscow KVANTOVAYA ELEKTRONIKA  
in Russian Vol 18 No 5, May 91 pp 610-612

[Article by V. K. Mezentshev and S. K. Turitsyn, Institute of Automation and Electrometry, Siberian Department, USSR Academy of Sciences, Novosibirsk]

UDC 681.7.068

[Abstract] Transmission of light pulses over optical fibers in the linear mode is considered, the detrimental effect of linear dispersion being usually minimized either by ensuring a zero second-order dispersion of radiation of the given wavelength so that the pulse

distortion will depend on the third-order dispersion or by use of a Kerr cell which will generate solitons in which dispersion is compensated by nonlinear steepening of the pulse front. In order to minimize the power necessary for generating such a nonlinear pulse, therefore, it is necessary to operate with radiation of wavelengths for which all dispersion effects, material-related and waveguide-related, will be minimum. This is shown to be achievable by utilizing nonlinearities of an optical fiber within the zero-dispersion region. The problem is analyzed theoretically on the basis of the P.K.A.Wai-C.R.Manyuk-H.H.Chen-Y.G.Lee equation (OPTICS LETTERS Vol 12, 1987) describing propagation of nonlinear pulses through single-mode fibers near a zero-dispersion point. This equation is, by appropriate change of variables, transformed into the dimensionless equation  $i\psi_z - i\psi_{ttt} + 2|\psi|^2\psi = 0$  where  $s = \text{sign}(\delta^3 k / \delta \omega^3)$  and then reduced to the Hamiltonian form  $i\psi_z = \delta H / \delta \psi^*$ . It has solutions which represent nonlinear pulses with a steady profile  $\psi(z, t) = \psi_0(\tau - z/v)e^{i\kappa z}$  ( $t$ -time,  $z$ -longitudinal space coordinate,  $\tau = t - z/v$ , denotes the "running" time,  $v$ -group velocity,  $v$ -velocity of pulse in a system of coordinates which moves at the group velocity,  $\kappa$ -propagation constant), the quantity  $\psi_0$  characterizing the waveform of such a soliton. Scale conversions  $\psi_0 \rightarrow s^{1/4}(3v)^{3/4}\psi_0$  and  $x = \tau/(3vs)^{1/2}$  reduce the nonlinear boundary-value problem of soliton structure with two parameters  $\kappa$  and  $v$  to a nonlinear boundary-value and also eigenvalue problem for only one parameter  $\mu = \kappa(3v)^{3/2}s^{1/2}$  playing here the role of a spectral parameter. The nonlinear term in this equation becomes negligible as  $|x| \rightarrow \infty$  and can be discarded so that, with  $\psi_0 \rightarrow A_s \exp[i\sigma]_{s \rightarrow \infty}$  as  $|x| \rightarrow \infty$ , this equation yields a cubic one for  $\sigma$ :  $\sigma^3 - 3\sigma + 2\mu = 0$ . Symmetry of the soliton solution  $[g < \infty] \psi_0(-x) = \psi_0^*(x)$  further simplifies the problem. A numerical solution of the boundary-value problem has revealed several heretofore unknown families of solitons. The steady ones resemble double solitons, solutions to the nonlinear Schroedinger equation, and describe interaction interaction of solitons in phase opposition with different numbers of zeros of their  $\text{Re } G(x) = [v^{3/4}\psi_0(xv^{1/2}/\sinh z)/3^{1/4}\sinh z \cdot \cosh z^{1/2}] \exp[-\text{lit}(\cosh z)/(3v)]^{1/2}$  function. The form of these double-hump solitons is universal so that the dependence of their integral characteristics on both  $v$  and  $\kappa$  can be readily determined. The power flux attending propagation of a soliton wave packet is calculated by integrating the Poynting vector over the fiber cross-section. On this basis has been estimated the peak power necessary for generating such solitons near a zero-dispersion point in single-mode quartz fibers. Figures 1; references 7.

# **Characteristics of Multichannel-Laser Radiation Pattern Formation by Beam Focusing**

927J0020F Moscow KVANTOVAYA ELEKTRONIKA  
in Russian Vol 18 No 5, May 91 pp 648-650

[Article by S. Yu. Denison, Ye. V. Zelenov, A. N. Safonov, V. M. Tarasenko, D. Yu. Filimonov, and Ye

A. Tserbakova, Scientific Research Center of Technological Lasers, USSR Academy of Sciences, Shatura (Moscow Oblast)]

UDC 621.373.826

[Abstract] An experimental study was made with an MTL-2 multichannel technological laser used for heat treatment, the problem being formation of its radiation pattern by beam focusing. The experiment was performed with a 500 W CO<sub>2</sub>-laser beam and interchangeably installed four KCl focusing lenses (focal length  $f$  = 223.9 mm, 322.2 mm, 391.3 mm, 521.7 mm). A compactor at the exit from the optical cavity reduced the aperture for the outgoing laser beam to one half. The dimensions of the successively larger light spots in the respective planes ("shelves") of minimum beam width were measured accurately within  $\pm 0.5$  mm on replicas made of acrylic glass, the locations of these planes relative to the focal plane of a given lens along the optical axis having been estimated by applying the laws of thin-lens geometrical optics to a presumably Gaussian laser beam. A close correlation ( $r > 0.95$ ) having been established, the data were subsequently processed in the linear approximation. The results reveal the sought dependence of the distance from the focal plane of that lens to the spot "shelf" on the distance from the exit aperture of the optical cavity to the plane of the focusing lens and on the focal length of that lens. Further experiments were performed pertaining to the laser-affected zone in a thus treated target. In the first experiment the laser beam was focused onto the target by placing the 391.3 mm lens at a distance of 43 cm from that target. With the lens in this position, the target was then moved across the laser beam for treatment at various rates ( $v$  = 1.55, 1.70, 1.90, 2.20 m/min). The beam was then defocused by moving the target 15 mm forward and 15 mm backward, its corresponding rates of transverse target movement in each of these two positions having been estimated on the basis of equal energy density. Defocusing was found not to change the depth but to increase the width of the laser-affected zone when the target was moving slowly and to decrease both equally when the target was moving fast. In the second experiment a spot of the same 5 mm width was produced with the different lenses, by placing them at the appropriate

distance each. With the target moving slowly (1.55 m/min), focusing the laser beam with the 521.7 mm lens was found to maximize the width and minimize the depth of the laser-affected zone. With the target moving fast (2.20 m/min), focusing with the 223.9 mm lens reduced the laser-affected zone to about one half its size and focusing with the 521.7 mm lens almost wiped it out completely. In the third experiment, with the 391.3 mm lens and with the target in the corresponding "shelf" (spot) plane, the geometrical dimensions of the laser-affected zone were measured and found to depend on the laser treatment parameters with both depth and width of this zone inversely proportional to the square root of the target velocity  $v$ . Figures 5; tables 2; references 2.

### Experimental Detection of Plasma Wave Barrier Brightening by Electron Beam

927J0060A Leningrad ZHURNAL TEKHNIЧЕСКОЙ ФИЗИКИ in Russian Vol 61 No 3, Mar 91 pp 49-52

[Article by I. A. Anisimov, S. M. Levitskiy, A. V. Opanasenko, L. I. Romanyuk, Nuclear Research Institute at the Ukrainian Academy of Sciences, Kiev]

[Abstract] The existence of opacity areas in inhomogeneous plasma - wave barriers which certain types of waves with certain parameters cannot penetrate without destroying the barrier - is discussed and the possibility of realizing the plasma wave barrier brightening, which ensures effective wave transmission through the barriers by means of regenerating the initial waves behind the barrier without changing the latter's properties, for an electromagnetic wave by enhancing the space charge wave (VPZ) in the electron beam inside the barrier and subsequently transforming it into an electromagnetic wave on the barrier output is demonstrated experimentally. The study was carried out at a discharge current of 0.4-1.5 A, a 70-150 V discharge in a uniform magnetic field of 0.01-0.02 T under an argon pressure in the discharge chamber of  $3 \cdot 5 \times 10^{-2}$  Pa. The electron beam was generated by a three-electrode electron gun. The experiment demonstrates the possibility of the plasma wave barrier brightening predicted theoretically. The cooperative processes which cause the electron beam's energy relaxation in the barrier suppress the above effect. Figures 5; references 11.

### Dibaryons and Thresholds

927J0025A Moscow FIZIKA ELEMENTARNYKH  
CHASTITS I ATOMNOGO YADRA in Russian  
Vol 22 No 3, May-Jun 92 pp 615-634

[Article by I. I. Starkovskiy, Leningrad Institute of  
Nuclear Physics imeni B. P. Konstantinov, USSR  
Academy of Sciences, Leningrad]

UDC 539.17

[Abstract] The status of research on dibaryon resonances in the  $I=1$ ,  $S=0$  channel of the nonstrange sector within the moderate  $s^{1/2}=1.88-3.02$  GeV energy range is reviewed, pertinent experimental data acquired over the 1983-90 period being analyzed generally for an association of dibaryons with thresholds. Phenomenological analysis of processes in the  $B=2$  system of two-particle and quasi-two-particle reactions is based on a unified multichannel approach, the  $T_J$ -matrix of total angular momentum covering nine simple reactions:  $NN \rightarrow NN$ ,  $NN \rightarrow \Delta N$ ,  $NN \rightarrow \pi d$ ;  $\Delta N \rightarrow NN$ ,  $\Delta N \rightarrow \delta N$ ,  $\Delta N \rightarrow \pi d$ ;  $\pi d \rightarrow NN$ ,  $\delta \rightarrow \Delta N$ ,  $\pi d \rightarrow \pi d$ . Wide diproton resonances have already been covered by energy-dependent and fixed-energy partial wave analyses. Here the data on 50-150 MeV wide diproton resonances are analyzed thus, assuming the existence of exotic wide diprotons (such an assumption being compatible with the bag model extended to multiquark systems, with the chiral soliton model, and with the standard dual model including fermions). New data on wide structures in the  $s^{1/2} > 2.3$  GeV energy range are particularly interesting on account of nontrivial anomalies in the energy and momentum dependence of variables such as cross-section and differential cross-section for elastic and inelastic reactions (scattering), resonance-like structures in this range having also been demonstrated by a new version of phase analysis. Reactions at or near the  $s^{1/2}=2.41$  GeV ( $^1G_4$  diproton), 2.7 GeV, and 2.9 GeV energy levels in this range are considered. Existence of long-lived dibaryons has not yet been ascertained, detection of at least one significant characteristic feature as an indicator of their existence being an experimental rather than theoretical problem. Dibaryons such as  $T^{++}$  and  $T^-$  in the narrow  $\Gamma < 20$  MeV range should be stable during strong interaction, inasmuch as their mass is below the  $\pi NN$ -threshold and isospin  $I_T=2$  conservation precludes the possibility of their decay in NN-reactions. Neither are their decays in electromagnetic interactions possible, owing to charge conservation. Their semi-lepton decays are closed, owing to the high-degree symmetry of the weak Hamiltonian in both  $d \rightarrow uW^-$  and  $u \rightarrow dW^+$  sectors. While a life longer than  $10^{-3}$  s does not seem to be likely even under optimum conditions, experiments involving interaction of a proton beam and a beryllium target in search of a  $T^-$  with a life longer than 1 ms have yielded results which indicate that the differential cross-section  $d^2\sigma/d\Omega dp$  for formation of this dibaryon is smaller than  $4 \times 10^{-43}$  cm<sup>2</sup>/(sr.MeV). The author thanks Ya.I. Azimov, R.A. Arndt, A.B. Kaydalov, L.A. Kondryatuk, B.Z. Kopelovich, T.-S.H. Lee, M.G. Ryskin, and A. Yokosawa for helpful discussions. Figures 13; Tables 4; references 75.

### Comparison Between Complete Systems of Levels in $^{106-116}\text{Cd}$ , $^{114-124}\text{Sn}$ , $^{122-130}\text{Te}$ Isotopes up to 2.5-3.0 MeV Excitation Energy

927J0044A Moscow YADERNAYA FIZIKA in Russian  
Vol 53 No 5, May 91 pp 1169-1179

[Article by A. M. Demidov and I. V. Mikhaylov, Institute of Atomic Energy imeni I. V. Kurchatov]

[Abstract] A comparison is made between the complete systems of levels in  $^{106-116}\text{Cd}$ ,  $^{114-124}\text{Sn}$ ,  $^{122-130}\text{Te}$  isotope chains up to 2.5-3.0 MeV excitation energy and their radiative properties, a common feature of these isotopes being that the  $Z$  number of Sn nuclei and the number 2 of protons in Te nuclei as well as the number 2 of proton holes in Cd nuclei are all magic numbers. Completeness of their systems of levels up to that range of excitation energy having been already established in earlier studies, this comparison covers: first levels with negative parity ( $J^\pi=3_1^-, 4_1^-, 5_1^-, 6_1^-, 7_1^-$ ), levels with  $N_\pi=3$  in Cd and Te isotopes, levels with  $N_\pi=3$  in Sn isotopes, two-phonon excitations, three-phonon excitations, levels with positive parity ( $J^\pi=4, 2$ ), and levels with  $J=1_1$ . The comparison reveals a partial similarity between the Cd and Te isotope chains, namely in the positions of some levels and in some radiative properties. The similarity is not complete, because the orbits of protons in Te nuclei are different than the orbits of proton holes in Cd nuclei. A comparison with the system of levels in Sn nuclei reveals that in these nuclei the positions of the lowest two-quasiparticle states with negative parity are remarkably independent of the energy gap in the Sn isotopes and that the excitation energy for two-quasiparticle neutron states with positive parity is also low. This indicates a weak coupling between the neutron system and the proton system in Sn nuclei, the proton system not even becoming excited when the lowest two-particle neutron states are. The positions of levels with a high degree of collectivity and most levels with  $2^+$  or  $4^+$ , however, do depend strongly on the magnitude of the energy gap as the latter increases in the Sn isotope chain. Figures 7; tables 3; references 12.

### Dynamics of Nonlinear-Schrodinger-Equation Soliton in Uniform Field in Adiabatic Approximation

927J0044B Moscow YADERNAYA FIZIKA in Russian  
Vol 53 No 5, May 91 pp 1292-1296

[Article by A. G. Lavkin, Central Scientific Research Institute of Scientific Measuring Apparatus, Saratov]

[Abstract] The behavior of the soliton of the nonlinear Schrodinger equation  $i\Psi_t + \Psi_{xx} + 2\Psi\Psi^2 = i\varepsilon F$  in a uniform external field  $F = A \sin \omega t$  is analyzed, in the adiabatic approximation  $\varepsilon \ll 1$ . Four integrodifferential equations for the rates of change  $d\eta/dt, d\xi/dt, d\mu/dt, d\delta/dt$  of the four dimensionless soliton parameters  $\eta$  (amplitude),  $\xi$  (displacement),  $\mu$  (velocity),  $\delta$  (phase) are written in accordance with the perturbation theory for analysis of the

soliton dynamics by the inverse scattering method. A numerical solution of that system of four equations reveals a dependence of both soliton amplitude ( $\eta$ ) and soliton velocity ( $\mu$ ) on the amplitude  $A$  of the external field. As the latter increases but not beyond the adiabatic limit, their dependence on it becomes more intricate while both continue to oscillate in phase opposition. The evolution of the soliton amplitude  $\eta(t)$  depends also on the frequency  $\omega$  of the external field, a higher frequency complicating the soliton excitation and dynamics. A monochromatic external field thus can, in the adiabatic approximation, complicate but not randomize the dynamics of such a soliton. The evolution of its amplitude  $\eta(t)$  depends also on its initial soliton velocity  $\mu_0$ . Raising its initial velocity makes the soliton more stable, inasmuch as its amplitude becomes a more regular function of time. This is confirmed by the  $\mu$ - $\delta$  (velocity-phase) diagram where the phase  $\delta$  has been normalized to a  $2\pi$  period. A high initial velocity makes the points of this diagram, which includes a Poincaré section, lie on closed regular curves forming an invariant torus. Lowering the initial velocity, on the other hand, makes the soliton dynamics pass through resonance. Figures 4; references 18.

#### New Approach to Treatment of Pontekorvo Reactions

927J0044C Moscow YADERNAYA FIZIKA in Russian Vol 53 No 5, May 91 pp 1410-1415

[Article by A. B. Kaydalov, Institute of Theoretical and Experimental Physics, Moscow]

[Abstract] Pontekorvo reactions  $\bar{p}d \rightarrow \pi^+p$ ,  $\bar{p}d \rightarrow K^0\Lambda(K^+\Sigma^-)$ , and  $\bar{p}^3\text{He} \rightarrow pn$  (B.M. Pontekorvo, ZHURNAL EKSPERIMENTALNOY I TEORETICHESKOY FIZIKI Vol 30, 1956) are analyzed by the method of Regge diagrams, considering that these reactions cannot proceed through interaction of an antiproton with quasi-free nucleons such as a deuteron or  $^3\text{He}$  nucleon but rather in the simplest way through absorption of one or both of the two produced  $\pi$ -mesons by the spectator nucleon. The cross-sections for these reactions depend largely on the behavior of the form factor, which describes the descent of a  $\pi$ -meson from the mass surface, and on the wave function of a deuteron on small distances. Both first and third of these three reactions are described by diagrams with exchange of respectively one and both of two baryon Regge poles in the  $t$ -channel, the first reaction being also described by a planar quark diagram according to the QCD model. Differential and total cross-sections for these reactions are then calculated accordingly, as functions of  $t$  ( $\text{GeV}^2$ ) and as functions of energy  $s^{1/2}$  ( $\text{GeV}$ ). The second of the three reactions is one with production of strange particles, exchange of Regge poles not being possible here so that another Regge diagram has been constructed for estimation of the reaction amplitudes. The author thanks C. Guaraldo and L.A. Kondratyuk for mentioning the Pontekorvo reactions and for many stimulating discussions. Figures 6; references 17

#### Measurement of Cross-Sections for Interaction of Reactor Antineutrino and Deuteron in Rovno Nuclear Electric Power Plant

927J0021A Moscow PISMA V ZHURNAL EKSPERIMENTALNOY I TEORETICHESKOY FIZIKI in Russian Vol 53 No 10, 25 May 91 pp 489-492

[Article by A. G. Vershinskiy, A. A. Meluzov, L. A. Mikaelyan, S. V. Nikolayev, M. D. Skorokhvatov, and A. V. Etenko, Institute of Atomic Energy Energy imeni I. V. Kurchatov, Moscow]

[Abstract] Interaction of electronic antineutrino and deuteron is being studied in the neutrino laboratory at the Rovno AES, measurements having been recently made which involved the antineutrino flux with a nominal thermal power of  $1375 \pm 2$  percent MW from the 440 MW VVER-440 water-cooled water-moderated power reactor. As the target was used a  $2985 \pm 3$  kg mass of 99.9 percent enriched heavy water containing  $1.796 \times 10^{29}$  nuclei, this  $D_2$ -detector filling a  $140 \times 140 \times 140 \text{ cm}^3$  volume chamber within graphite walls surrounded by a cadmium shield. Reactions were recorded on the basis of the neutron count only, by  $196^{\text{Au}}$  counters forming an array of 14 rows of 14 rods uniformly spaced 10 cm apart in the heavy water. Noise associated with cosmic rays was suppressed by anticoincidence scintillation plates surrounding the detector, between the cadmium shield and a polyethylene jacket, also by containers with a liquid scintillator substance forming an "umbrella" above the detector. Events were sampled by amplitude and repetition of pulses within a 1500  $\mu\text{s}$  time window. Only single events were used for recording the  $\bar{\nu}_e + d \rightarrow n + p + \bar{\nu}_e$  (neutral-current) process, this process producing one neutron in its final state. Double and single events were used for recording the  $\bar{\nu}_e + d \rightarrow n + p + e^+$  (charged-current) process, this process producing two neutrons but one of which may not always have been detected. The recording efficiency and the upper bound of measurement error were established experimentally, using a  $\text{SbBe}$  source of neutrons with 24 keV energy and a  $\text{PuLi}$  source of neutrons with approximately 200 keV average energy. Measurements were made with the reactor turned off for background count and with the reactor turned on at constant power levels for background + antineutrino effect count, the total number of interaction events in the detector target along neutral-current (nc) channels and along charged-current (cc) channels being proportional to the reactor power. The cross-sections for antineutrino-deuteron interactions were then calculated according to the relation  $N_{nc,cc} = WN_d\sigma_{nc,cc}/4\pi R^2 E_f$  ( $W$  denoting the reactor power,  $N_d$  denoting the number of nuclei in the target,  $E_f = \Sigma \alpha_i E_i$  denoting the average energy absorbed in the reactor core during one fission, and  $\sigma = \Sigma \alpha_i \sigma_i$  denoting the average cross-section, dependent on the isotopic content of the fuel with the contributions of isotopes to the total number of fissions characterized by the coefficients  $\alpha_i$ :  $i=5$  for  $^{235}\text{U}$ ,  $i=9$  for  $^{239}\text{Pu}$ ,  $i=8$  for  $^{238}\text{U}$ ,  $i=1$  for  $^{241}\text{Pu}$ ). There were accordingly found to have been recorded  $N_{nc} = 500 \pm 85$  and  $N_{cc} = 216 \pm 25$  interactions. The thus determined cross-sections for interactions

$\sigma_{nc}=2.71 \times 10^{-44} \text{cm}^2/\text{fission}$  (with  $\pm 0.46$  random error and  $\pm 0.11$  systematic error) and  $\sigma_{oc}=1.17 \times 10^{-44} \text{cm}^2/\text{fission}$  (with  $\pm 0.14$  random error and  $\pm 0.07$  systematic error), corresponding to an isotopic content of 59.9 percent  $^{235}\text{U}$ +28.1 percent  $^{239}\text{Pu}$ +7.4 percent  $^{238}\text{U}$ +4.6 percent  $^{241}\text{Pu}$ , agree closely with the predicted  $(2.96 \pm 0.12) \times 10^{-44} \text{cm}^2/\text{fission}$  and  $(1.08 \pm 0.07) \times 10^{-44} \text{cm}^2/\text{fission}$ . The authors thank Yu.V. Gaponov and S.A. Fayans for helpful discussions of theoretical problems, also colleagues at the laboratory for assistance in preparation of the experiment. Figures 1; tables 1; references 5.

#### Deformation of $^{74-80}\text{Kr}$ Nuclei and Their Moments of Inertia

127J0051A Leningrad IZVESTIYA AKADEMII NAUK  
SSSR: SERIYA FIZICHESKAYA in Russian Vol 55 No  
1, Jan 91 pp 30-33

[Article by I. Kh. Lemberg, I. A. Mitropolskiy, Leningrad Nuclear Physics Institute imeni B. P. Konstantinov at the USSR Academy of Sciences]

UDC 539.144

[Abstract] Abrupt changes in the nuclear state structure with changes in the number of protons or neutrons and angular momentum in  $A=70-80$  nuclei, e.g., high values of the  $2_1^+$  level energy and a high collectivization of  $E2$  transitions in even-numbered krypton isotopes, are discussed. A self-consistent cranking model is developed and used to calculate the energy of the levels and probabilities of  $E2$  transitions in the fundamental rotational band of krypton's even-numbered isotopes. Specific calculations were made for  $^{74}, ^{76}, ^{78}, ^{80}\text{Kr}$  isotopes;  $^{72}\text{Kr}$  was omitted for lack of experimental data while  $^{82}\text{Kr}$  was not used due its proximity to the  $N=50$  closed electron shell. The magnitude of deformation in the fundamental state of these nuclei is discussed on the basis of several approaches. It is noted that the deformation parameters at which the best description of the level energies is attained are consistent with the values obtained by the shell approximation method and correspond to the  $E2$  transition probabilities observed for  $^{78}\text{Kr}$  and  $^{80}\text{Kr}$ ; in the case of  $^{74}\text{Kr}$  and  $^{76}\text{Kr}$ , the experimental values of  $B(E2)$  exceed noticeably the theoretical figures. Figures 1; tables 1; references: 5 Western.

### Propagation of Light Pulse Through Tunnel-Coupled Nonlinear Optical Waveguides

927J0019E Moscow KVANTOVAYA ELEKTRONIKA in Russian Vol 18 No 6, Jun 91 pp 758-761

[Article by A. I. Maymistov, Moscow Institute of Engineering Physics]

UDC 621.372.8.029.7

[Abstract] Propagation of a light pulse through two tunnel-coupled nonlinear fiber-optic waveguides is analyzed by the method of variational calculus on the basis of a system of two equations describing its propagation. The two equations are converted into two Euler-Lagrange equations, with an appropriately formulated Lagrangian. Calculation of the variational derivatives leads to a system of three ordinary differential equations. Two two of them yield the momentum integral and are then reduced to two equations describing the kinetics of soliton formation. Assuming for simplicity that the two waveguides are identical, in terms of equal propagation constants, an analytical solution is obtained for the two extreme cases of strong and weak tunnel coupling. In the first case a light pulse is found to propagate as it does through a nonlinear integrated-optics directional coupler. In the second case the pulse will be widened owing to the dispersion of group velocities, unless the initial pulse power is sufficiently high. Then a quasi-soliton will form and propagate as it does through strongly tunnel-coupled waveguides. The author thanks K.S. Karplyuk and F.Kh. Abdullayev for suggesting this problem, also K.I. Gritsay and S.V. Snezhko for helpful comments. References 25.

### Luminescence of Absorption Domains (Autowaves) in CdS

927J0021B Moscow PISMA V ZHURNAL EKSPERIMENTALNOY I TEORETICHESKOY FIZIKI in Russian Vol 53 No 10, 25 May 91 pp 496-499

[Article by V. A. Stadnik, Institute of Solid-State Physics, USSR Academy of Sciences, Chernogolovka]

[Abstract] An experimental study of absorption domains in CdS semiconductor crystals was made by the luminescence method, its purpose being to determine their maximum temperature and the temperature in their region of maximally efficient light-to-heat conversion along with the corresponding absorption coefficients. The luminescence spectra of these domains in 1.3-2.0 mm thick CdS specimens were recorded with a 5-10  $\mu$ m spatial resolution and a 1 meV spectral resolution, upon excitation by a beam of second-harmonic radiation (2.33 eV photon energy) from a quasi-CW YAG:Nd-laser operating either in the continuous-wave mode or with Q-switching and pulse width regulation over the 0.2-25  $\mu$ s range at an average power level of 500-600 mW. The incident light beam was oriented along the optical axis of

a crystal. Measurements were made with a multichannel spectrum analyzer including an MDR-12 monochromator and an RM-3315 oscillograph, both coupled to an IBM PC-AT 286 personal computer. First was measured the luminescence spectrum of such a crystal in the initial domainless state, excited by a 30 mW laser beam. Then were measured the luminescence spectra of this crystal with stationary absorption domains forming at its front face, upon excitation by a 445 mW laser beam and upon excitation by a 505 mW laser beam. Increasing the power of the incident laser beam was found to widen the luminescence spectrum of such localized domains, like that of a quasi-homogeneous crystal, with an attendant red shift (toward lower photon energy) of the maximum intensity. The farthest red shift of the maximum intensity was recorded when these domains were stable, already slight oscillations of such domains causing reverse blue shift of the maximum intensity of their luminescence. At the rear face of a crystal were found to have formed stationary and traveling absorption domains. The luminescence spectrum of these domains was characterized by an emission line 30-50 percent wider than the emission line of domains at the front face and with the maximum intensity at a wavelength close to the excitation wavelength, its contour remaining almost constant and its location shifting very little as the excitation power was varied. Inasmuch as in this experiment the concentration of photoexcited charge carriers was low, never exceeding  $10^{16}$ , the maximum temperature of absorption domains could be determined from the spectral location of the emission line. The maximum temperature of domains localized at the front face of a CdS crystal was thus found to lie within the 380-420 K range. The maximum temperature of localized and traveling absorption domains forming at the rear face of a Cd crystal was found to be not higher than 390-400 K, the temperature of the active region of light-to-heat conversion lying within the 330-370 K range. Calculations based on Urbach's rule and a linear temperature dependence of the energy gap width have yielded an exponential temperature dependence of the absorption coefficient, indicating an analogy to the kinetics of combustion. The author thanks V.B. Timofeyev for support the study, V.D. Kulyakovskiy and M.V. Lebedev for helpful discussion of the results. Figures 2; references 6.

### Change in Optical Properties of Leucosapphire Caused by Hot Plastic Deformation

927J0024B Leningrad FIZIKA TVERDOGO TELA in Russian Vol 33 No 4, Apr 91 pp 1173-1177

[Article by I. I. Afanasyev, L. K. Andrianova, V. N. Vetrov, and B. A. Ignatenko, State Institute of Optics imeni S. I. Vavilov, Leningrad]

UDC 548.552:539

[Abstract] An original experimental study of uniaxial crystals was made concerning the effect of nonuniform

hot plastic deformation on their optical indicatrix, circular disks of Z-cut leucosapphire single crystals having been hot formed for this purpose into hemispherical shells. The disks were formed into such shells with a 72 mm inside base diameter and a 19 mm high riser. Slip and structural transformations were monitored with a PKS-125 optical polariscope which, using a source of diffuse 550 nm light, recorded birefringence and interference patterns of the menisci during the deformation process. In circularly polarized light the slip lines and the interference isochromes were found to form a pattern with a third-order axis, indicating a 3m point symmetry of original leucosapphire single crystals. Examination of surfaces cut parallel to the Z-axis revealed a nonparallel fanning out of the optical axis. Hot plastic deformation of a uniaxial crystal thus evidently modifies the geometrical pattern of its optical properties so that it becomes one intermediate between their pattern in a natural single crystal and their pattern in a polycrystalline structure, the degree of this modification being controllable by the deformation process. Figures 2; references 6.

#### Optical Waveguide Electrooptic RF Field Transducer

927J0060B Leningrad ZHURNAL TEKHNIЧЕСКОY FIZIKI in Russian Vol 61 No 3, Mar 91 pp 161-164

[Article by V. K. Gorchakov, V. V. Kutsayenko, V. T. Potapov, Radio Engineering and Electronics Institute at the USSR Academy of Sciences, Fryazino, Moscow oblast]

[Abstract] Pockels' electrooptic effect is examined for the purpose of developing new instruments for measuring the parameters of RF fields. To this end, electrooptic light modulation in a  $(\text{Bi}_{12}\text{SiO}_{20})$  bismuth silicate crystal in a microwave (SVCh) field is examined in order to develop an optical waveguide transducer in which optical radiation is transmitted over optical fibers. Bismuth silicate's advantages over other crystals due to its cubic structure are outlined. An analysis of the polarized light modulation shows that for detecting RF fields, it is expedient to ensure modulation in the optical square law detector mode in which case the RF pulse envelope is recorded by an inertial photodetector. A

transducer prototype was manufactured and investigated. The study made it possible to observe both a qualitative and quantitative consistency between the theory and the prototype's readings and revealed a square law dependence of the depth of light modulation on the field in low-frequency and microwave fields. The transducer may be used as the basis of an instrument system for monitoring strong pulsed fields. The authors are grateful to S.G. Chigarev for help with experimental verification of the transducer in the microwave field. Figures 4; references 5: 2 Russian, 3 Western.

#### Fiber Optic Sensor For Magnetic Field Transducer

927J0060C Leningrad ZHURNAL TEKHNIЧЕСКОY FIZIKI in Russian Vol 61 No 3, Mar 91 pp 175-177

[Article by S. N. Antonov, Radio Engineering and Electronics Institute at the USSR Academy of Sciences, Fryazino, Moscow oblast]

[Abstract] The use of, and outlook for, magnetic field transducers with a fiber optic (VS) sensor is discussed. These transducers' advantage is the possibility of utilizing the optical anisotropy induced by the regular bend as a result of the optical fiber winding, i.e., realizing a longitudinal light wave phase synchronism given a spatial periodic modulation of the medium's dielectric constant caused by the magnetic field. The sensor configuration which makes it possible to select beforehand the fiber optic coil diameter which ensures synchronism at a given wavelength is presented. The design was used to make a magnetic field transducer sensor prototype with a traditional optical train with a 1 mW He-Ne laser, a polarizing filter, a sensor, a polarizing prism, and two silicon photodetectors. The sensor was placed in a 1 kHz magnetic field. The study demonstrates that the signal corresponding to a 90° polarization plane rotation on the sensor output is observed at a magnetic field of about 800 Oe while that corresponding to signal/noise ratio equal to unity - at  $10^{-2}$  Oe. The author is grateful to A.N. Bulyuk and V.M. Kotov for help with the experiment and a group of colleagues under the leadership of G.A. Ivanov for making the optical waveguide. Figures 2; references 3: 2 Russian, 1 Western.

**Production of Hot Electrons in Open Traps  
During Electron-Cyclotron-Resonance Heating  
With Longitudinal Injection of Microwave Power**

927J0028A Moscow FIZIKA PLAZMY in Russian  
Vol 17 No 7, Jul 91 pp 771-784

[Article by V. A. Zhiltsov, A. A. Skovoroda, A. V. Timofeyev, K. Yu. Kharitonov, and A. G. Shcherbakov, Institute of Atomic Energy imeni I. V. Kurchatov]

UDC 533.951.8

[Abstract] An experiment involving electron-cyclotron-resonance (ECR) heating of a plasma was performed in the OGRA-4 facility, for a study of hot electrons (with an energy higher than the mean energy of the principal plasma component) produced in the process. The apparatus consisted of a superconducting magnet system of the baseball type with a single open trap, the magnetic field intensity here passing through its minimum, and with an approximately 2:1 length-to-width ratio of the plug. The magnetic field was made sufficiently strong for electron-cyclotron resonance to occur in the trap upon injection of 8 mm radiation from a 200 kW gyrotron in a pulse of 50 ms duration. Earlier studies have already revealed that factors strongly influencing the buildup of a hot electron population include the magnitude of electromagnetic oscillations, the transverse motion of plasma electrons, the finite width of the injected microwave beam, the presence of a microwave background noise, and the Doppler effect. Earlier experiments in the TARA apparatus have also revealed that excessive "superheating" of electrons in a stabilizer can weaken their interaction with electromagnetic oscillations in the trap and consequently make such a stabilizer cease to function. This effect was avoided in the OGRA-4 facility, as verified by readings taken with bolometers. Plasma parameters measured in this experiment were: plasma density in the trap center, volume of cold plasma and characteristic diameter of region containing cold electrons, their concentration and mean energy, volume of warm plasma and characteristic diameter of region containing warm electrons (such electrons being easily retained in a magnetic well), their concentration and mean energy, volume of hot plasma and characteristic diameter of region containing hot electrons, their concentration and mean energy of hot electrons, maximum beta-factor at a baseball current level of 1.3 kA, mean lifetime of cold, warm, and hot electrons, mean energy of ions, plasma potential, and longitudinal plasma current. Theoretical analysis and interpretation of the data on the dynamics of hot electrons in such an open trap as they are drawn from the reservoir of cold and warm electron populations is based on a model which combines ECR heating of a plasma and propagation of electromagnetic waves through a plasma, taking also into account the Doppler effect and the attenuation of electromagnetic waves by hot electrons. The amplitude of the microwave field at the site of electron-cyclotron resonance is assumed to be sufficiently large for the energy distribution of hot

electrons  $f(\epsilon)$  to evolve in accordance with the quasi-linear diffusion equation  $\delta f / \delta t - (\delta D / \delta \epsilon)(\delta f / \delta \epsilon) = q$ . Two additional parameters are introduced for the analysis: initial longitudinal energy of warm electrons, prior to their acceleration, and fraction of the total injected microwave power spent on heating up cold or warm electrons. The results indicate the maximum electron energy and the maximum plasma energy attainable in open traps, how these parameters can be controlled, and how ECR-heating can be most efficiently used for stabilizers in ambipolar traps. The authors thank A.V. Zvonkov for discussions. Figures 10; tables 1; references 26.

**Anomalous Large Cathode Region in Molecular  
High-Pressure Plasma**

927J0028B Moscow FIZIKA PLAZMY in Russian  
Vol 17 No 7, Jul 91 pp 868-873

[Article by S. Ya. Bronin, A. A. Vanin, M. G. Kasparov, V. M. Kolobov, A. V. Mokhov, and A. P. Nefedov, Institute of High Temperatures, USSR Academy of Sciences; Institute of Energy Problems in Conservation Problems, UkSSR Academy of Sciences]

UDC 533.9.082.76

[Abstract] An experiment with a molecular plasma was performed under conditions favoring formation of an anomalously large cathode region and thus facilitating the determination of its electric potential profile and temperature profile on the basis of point-by-point measurements. Such a plasma was generated in a propane-air flame, with 5 percent excess fuel in the mixture. An additive containing easily ionizable sodium, namely  $\text{Na}_2\text{CO}_3$ , was injected by a pneumatic sprayer into the inner jet of the Mecker burner. The burner barrel served as the anode. The cathode was a copper cone with a 60° vertex angle, its tip rounded to a 0.8 cm radius and its axis of symmetry collinear with that of the burner. The interelectrode gap between the tip of this conical cathode and the edge of the burner-anode was 3 cm wide. The cathode was grounded through the low resistance of a digital voltmeter used as current measuring device and a high potential in the kilovolt range was applied to the anode. First were measured the current-voltage characteristics of discharges in propane combustion products (73 percent  $\text{N}_2$ , 16 percent  $\text{H}_2\text{O}$ , 11 percent  $\text{CO}_2$ ) in air under atmospheric pressure, the results indicating existence of an anomalously large region of charge separation with an about 1 cm thick space charge layer at the cathode. Estimates based on these measurements are shown to validate theoretical estimates based on numerical solution of a system of five equations of hydrodynamics applicable to a cathode region with a boundary layer so thin as to be negligible: 1) Poisson's equation for the electric field intensity; 2) two equations for the electron current density and for the ion current density

respectively, each current consisting of a drift component and a diffusion component; 3) two equations of charge balance during ionization and recombination. Subsequent temperature and thermal flux measurements made with three Chromel-Alumel thermocouples in key positions yielded temperature profiles in the cathode region, profiles closely approaching those estimated theoretically estimated on the basis of a numerical solution of the approximate MacDaniel equation for the electron temperature in a multicomponent gaseous mixture of combustion products (I. MacDaniel; "Collision Processes in Ionized Gases"). Such a good agreement between theoretical and experimental data raises the expectation that similar point-by-point probing of the cathode region in high-pressure molecular plasmas will yield as reliable results when the space charge layer is sufficiently thick. Figures 4; tables 1; references 13.

#### **Anomalous Plasma Transport in Neoclassical Modes Due to Pressure Gradient**

927J0043A Moscow FIZIKA PLAZMY in Russian  
Vol 17 No 6, Jun 91 pp 643-649

[Article by V. P. Lakhin, Institute of Atomic Energy imeni I. V. Kurchatov]

UDC 533.951

[Abstract] Anomalous transverse plasma mass and energy transfer along magnetic surfaces in a tokamak and thus with a pressure gradient is analyzed theoretically on the basis of "neoclassical" magnetohydrodynamics. Averaging the magnetic field metric over oscillations yields for a tokamak a system of four nonlinear equations, the last one reducing to a continuity equation in the case of a uniform temperature distribution with negligible perturbations. Bootstrap currents, Weyr pinch, and damping of poloidal plasma rotation are included, but negligible resistance-redistribution instability due to curvature of the magnetic field is disregarded. Collisionless anomalous heat conduction by plasma electrons due to randomization of the magnetic field near magnetic surfaces is considered, its dependence and also the dependence of the plasma diffusion coefficients on the local plasma parameters being calculated by two methods: one based on invariance of those nonlinear equations under scaling transformations and one based on the theory of mixing length in turbulent flow. The results obtained by both methods for a toroidal collisionless plasma are consistent. For a toroidal impact plasma, however, they yield different ratios of the plasma relaxation frequency to the electron collision frequency. The authors thank S.Ye. Sharapov for helpful discussions and A.B. Mikhaylovskiy for support. References 16.

#### **Limitation of Microwave Radiation Pulse Duration in Oscillators With Microsecond-Pulse Relativistic Electron Beams**

927J0043B Moscow FIZIKA PLAZMY in Russian  
Vol 17 No 6, Jun 91 pp 751-755

[Article by S. N. Voronkov, O. T. Loza, and P. S. Strelkov, Institute of General Physics, USSR Academy of Sciences]

UDC 621.385

[Abstract] An experimental study of microwave oscillators with relativistic electron beams carrying microsecond current pulses was made, concerning the feasibility of eliminating known factors which limit the duration of microwave pulses and thus cause cutoff of microwave generation. The experiment was performed with a 500 keV electron beam carrying a current of 3 kA in pulses of 1  $\mu$ s duration in a carcinotron, designed for generating the  $E_{02}$  mode at 3 cm wavelength and for mode selection by the cyclotron absorption method. The possibility of microwave breakdown at the carcinotron walls was appreciably diminished by making the diameter of the electrodynamic structure twice as large as in a carcinotron designed for generating the  $E_{01}$  mode. Between the 36 mm in diameter cathode and the carcinotron entrance was placed a 42 mm in diameter graphite diaphragm, both the cathode and the diaphragm 10 cm behind being situated in a uniform 14 kHz alternating magnetic field. This magnetic field could be regulated by tapering its intensity from the magnitude at the cathode down along the path of the electron beam so that the initial diameter of the latter inside the carcinotron could be in this way be enlarged from 36 mm up to 40 mm. The tests revealed a dependence of the microwave power and thus of the microwave pulse amplitude on the intensity of the magnetic field with a characteristic minimum exactly at electron-cyclotron resonance, confirming operation of the carcinotron in the mode selection mode. They furthermore revealed plasma formation at the collector upon axisymmetric shrinkage of the electron beam here to a 6 cm diameter at a beam current of 1 kA, and plasma formation at the diaphragm upon bombardment of its periphery by the electron beam. Plasma was also found to be forming upon bombardment of the oscillator walls by diverging beam electrons. The width of the electron beam was changing in time, this process significantly influencing the duration of the generated microwave pulse. An analysis of the results indicates no likelihood of the microwave pulse duration being limited by microwave breakdown in a magnetic field of intensity lower than the optimum, inasmuch as lowering the magnetic field intensity already causes the microwave pulse duration as well as amplitude to decrease. In order to lengthen the microwave pulse duration, it is therefore necessary to either stabilize the electron beam diameter or to design the oscillator with sufficiently large cross-sections but

with low sensitivity to changes in the electron beam diameter. Figures 1; references 6.

### Formation of Wide High-Current Electron Beam of Microsecond Duration

927J0043C Moscow FIZIKA PLAZMY in Russian  
Vol 17 No 6, Jun 91 pp 741-745

[Article by E. N. Abdullin, S. Ya. Belomytsev, S. P. Bugayev, S. N. Gorbachev, V. M. Zaslavskiy, V. P. Zorin, B. M. Kovalchuk, S. V. Loginov, Yu. N. Matyukov, R. M. Rasputin, V. S. Tolkachev, and P. M. Shchanin, Institute of High-Current Electronics, Siberian Department, USSR Academy of Sciences]

UDC 537.533.3

[Abstract] A feasibility study was made concerning formation of an electron beam for controlled thermonuclear fusion, an electron beam with a rectangular cross-section carrying a current about as high as the peak diode current in a pulse of microsecond duration without a guiding external magnetic field and with "fast" storage in the supply circuit. A vacuum diode as source of a 500-600 keV electron beam with a  $25 \times 100 \text{ cm}^2$  cross-section carrying a current of 50-70 kA in a pulse of about 1  $\mu\text{s}$  duration was built on the basis of a computer-aided design using the "Poisson" program package, the problem of formation of such an electron beam in a diode with an intrinsic magnetic field having accordingly been treated as a two-dimensional problem and solved by the method of iterations with respect to space charge relaxation. The thus designed nominal vacuum diode has a 25 cm wide cathode with a 20 cm wide active surface and a circular anode with a 53 cm long radius, the distance between them along the axis of symmetry being 6.3 cm long. A voltage of 500 kV applied across this diode generates a current of 47 kA, its distribution over the anode surface deviating by about 30 percent from a uniform one. A reduction of the voltage to 300 kV lowers the current to 22 kA, approximately in accordance with Child's law, but widens the beam at the anode surface. A return of the voltage to 500 kV after a plasma layer has formed at the anode raises the current to 82 kA but narrows the beam at the anode surface. The experiment was performed with a low-inductance Marx generator consisting of eight stages, the capacitor in each stage consisting of three segments with a discharger each and the generator walls being vacuum sealed so as that the cathode could be placed directly behind the last stage without a vacuum spacer. The cathode was made of stainless steel and only 18 cm wide. It was tested with various kinds of emitting surface layers and found to perform best when covered with 81-88 cm long strips of velvet or carbon-graphite felt. An emitter in the form of 144 graphite fins spaced 5 cm apart in 4 rows of 36 and projecting 2 cm from the base surface was also tested, but the performance of the diode with such a cathode became somewhat unstable. The anode was a either a stainless steel disk or a vacuum-tight foil (30  $\mu\text{m}$  thick stainless

steel, 30  $\mu\text{m}$  thick titanium, 50  $\mu\text{m}$  thick Al-Mg2 alloy) on a  $25 \times 100 \text{ cm}^2$  large supporting exit window with 85 percent geometrical transparency. The diode current calculated with correction for a rise of the electric field intensity at the cathode edges exceeded its  $I_{3/2}$  magnitude according to Child's law. The ratio of these two magnitudes remained almost constant as the voltage is raised, an indication of an almost negligible effect of the intrinsic magnetic field in the diode and of the relativistic factor on the beam space charge in the diode. The current, measured with a Rogowski loop and a set of shunts, was higher than the nominal current and especially so in the range of lower voltages. The ratio of measured current to the  $I_{3/2}$  current according to Child's law depended appreciably on the applied voltage but not significantly on the diode geometry (interelectrode distance). A higher than nominal current cannot be explained by movement of the cathodic plasma and is more likely attributable to partial compensation of the negative space charge by ions of gas evolving at the anode and thus to a role of anodic processes in formation of the electron beam. This is further evidenced by the results of energy measurements made with a set of calorimeters, these measurements revealing an energy distribution over the beam cross-section much more nonuniform than according to calculations based on absence of ions in interelectrode space. Figures 5; references 7.

### Maximum Electric Field Intensity in Plasma Wake Wave

927J0022A Moscow PISMA V ZHURNAL  
EKSPERIMENTALNOY I TEORETICHESKOY  
FIZIKI in Russian Vol 53 No 11, 10 Jun 91 pp 540-544

[Article by S. V. Bulanov, V. I. Kirsanov, and A. S. Sakharov, Institute of General Physics, USSR Academy of Sciences, Moscow]

[Abstract] Acceleration of particles by a plasma wake wave is considered, such a wave being generated by a laser pulses or by a bunch of relativistic electrons. The performance of such a high-energy accelerator is analyzed for maximum attainable electric field intensity, known to be much higher here than in a vacuum chamber (where it is limited by breakdown at the walls). The theoretical part of this analysis is based on the system of applicable Vlasov-Poisson equations, the solution indicating that thermal scatter of electrons facilitates their capture by a plasma wake wave and thus lowers the maximum electric field intensity. Expressions are obtained for the maximum electric field intensity in an electron plasma under these conditions: in a plasma with an isotropic electron temperature  $E_{\text{max}} \approx \kappa(T_e/mc^2)^{-1/4}$  when  $1 \gg T_e/mc^2 \gg \gamma^{-2}$  ( $\kappa = mc\omega_p/e$ ,  $\omega_p$  - plasma frequency corresponding to quiescent electron concentration,  $T_e$  - electron temperature,  $m$  - electron mass,  $e$  - electron mass,  $c$  - speed of light,  $\gamma = [1 - (v_{ph}/c)^2]^{-1/2}$ ,  $v_{ph}$  - phase velocity of plasma wake wave) and in plasmas with anisotropic electron temperatures,  $E_{\text{max}} \approx$

$\kappa(T_{e,l}/mc^2)^{-1/4} \log[\gamma^{1/2}(T_{e,l}/mc^2)^{1/4}]^{1/2}$  when  $l \gg T_{e,l}/mc^2 \gg \gamma^2$ ,  $T_{e,l}/mc^2$  (high longitudinal electron temperature  $T_{e,l}$ ),  $E_{max} \approx \kappa(T_{e,l}/mc^2)^{-1/2}$  when  $l \gg T_{e,l}/mc^2 \gg T_{e,t}/mc^2, \gamma^2$  (high transverse electron temperature  $T_{e,t}$ ). Further calculations indicate that excitation by a relativistically strong laser pulse so that the phase velocity  $v_{ph}$  of the wake wave is equal to the group velocity  $v_{gr}$  of the leading pulse edge and thus  $\gamma = \omega_0/\omega_p$  ( $\omega_0$ -carrier frequency of laser field) can induce an electric field of an intensity either up to  $E_{max} = \kappa\gamma$  and thus much higher than in the wake of a steady wave when the laser pulse is a quasi-square one with a steep leading edge corresponding to a rise time  $\delta\tau < (qga_1)^{-1}(a_1 = eE_1/m\omega_0 c)$  dimensionless amplitude of laser pulse along its leading edge) and  $a_1 < \gamma^{1/2}$  or up to  $E_{max} \approx k(\omega_p \delta\tau)\gamma^2$  when the laser pulse has a mild leading edge corresponding to a rise time  $\delta\tau > (\omega a_1)^{-1}$ . A numerical analysis based on this model of particle acceleration in a plasma chamber indicates the feasibility of inducing, with an ultrashort laser pulse, a transient electric field of  $E_{max} \approx 4$  GV/cm intensity in a plasma with a  $n_0 = 10^{19} \text{ cm}^{-3}$  electron concentration. Figures 3; references 9.

#### Development of Diffusion Processes During Plasma-Arc Deposition of Coatings

927J0042B Novosibirsk SIBIRSKIY FIZIKO-TEKHNICHESKIY ZHURNAL in Russian No 1, Jan-Feb 91 pp 105-108

[Article by S. A. Rebut and A. P. Kudinov, Institute of Metallurgy, Ural Department, USSR Academy of Sciences, Sverdlovsk]

UDC 621.793

[Abstract] An experimental study of diffusion processes during plasma-arc deposition of nickel coatings on

Armco iron and on grade-40 carbon steel was made, for which such 0.3 mm thick coatings for this study were deposited with a plasmatron on 20 mm thick and 28 mm diameter disks after the latter had been polished by shot blasting. The distribution of chemical elements across the entire substrate-coating structure and especially across the transition layer was monitored by microanalysis with a Comebax apparatus using a 4  $\mu\text{m}$  wide electron probe. The mean temperature of the substrate surface was throughout the entire deposition process maintained at 873 K and thus above the Ni — Fe diffusion activation temperature, the temperature of the substrate 3.5 mm below the surface having risen to 393 K only. Movement of the plasmatron relative to the thermocouple stuck to the substrate surface caused not wider than  $\pm 100$  K fluctuations of the temperature readings. The diffusion zone within the transition layer was found to be almost equally wide, about 13  $\mu\text{m}$  wide, on all disks. For an analysis and interpretation of the experimental data from the standpoint of the theory of plasma-arc coating and attendant diffusion kinetics, the relevant diffusion coefficients and the vacancy flux have been calculated according to the Boltzmann-Matano equation and the Onsager equation respectively. A comparison is also made with other methods of coating, specifically the gas-flame method. The results of this analysis indicate that during deposition of a nickel coating on iron (steel) development of the diffusion process takes a time very much longer than the time of interaction of the two materials, namely the time taken by nickel droplets to spread over the substrate surface and subsequently solidify. Thermal diffusion evidently plays an appreciable role in the process. No anomalies have been detected, widening of the diffusion zone being attributable to both thermal diffusion and structural imperfection. Figures 2; references 11.

### Acoustic Spectrum Modification of Piezocrystal Wafers Using Superconducting and Metallic Coats

927J0058A Moscow KRISTALLOGRAFIYA in Russian Vol 36 No 4, Jul-Aug 91 pp 828-833

[Article by V. I. Alshits, V. N. Lyubimov, Crystallography Institute at the USSR Academy of Sciences and Physics-Chemistry Scientific Research Institute imeni L. Ya. Karpov]

UDC 537.312.62

[Abstract] The possibilities of modifying the acoustic characteristics of piezomagnetic and piezoelectric materials with the help of superconducting or metallic coats are investigated. To this end, piezocrystal wafers with a thin (compared to the wavelength) superconductor or metal layer applied to one or both faces are examined. Characteristic changes in the acoustic spectrum due to the presence of the coats and their transition from the superconducting to the normal metallic state are studied. The spectra of surface acoustic waves and transverse volume acoustic waves in piezomagnetic and piezoelectric crystals wafers are recorded. These data show that the use of superconducting and metallic coats on piezocrystal wafer faces modifies the acoustic spectrum of surface and volume acoustic waves and makes it possible to obtain a broad diversity of acoustic fields in such crystals. It is noted that the spectrum changes rather sharply with changes in the phase state of superconducting coats on piezomagnetic crystals. Figures 1; references 7: 6 Russian, 1 Western.

### Steady-State Josephson Effect in High- $T_c$ Superconductor Junctions

927J0029A Kharkov FIZIKA NIZKIKH TEMPERATUR in Russian Vol 17 No 6, Jun 91 pp 692-702

[Article by B. A. Aminov, L. Roshta, Ya. G. Ponomarev, and M. V. Sudakova, Moscow State University imeni M. V. Lomonosov; TaSSR Institute of Engineering Physics imeni S. U. Umarov, Dushanbe]

UDC 538.945

[Abstract] An experimental study of the Josephson effect in high- $T_c$  superconductor junctions was made by a method involving formation of a microcrack at liquid-helium temperature (J.-S. Tsai, Y. Kubo, and J. Tabuchi; JAPANESE JOURNAL OF APPLIED PHYSICS Vol 26 No 5, 1987). Tests were performed on polycrystalline  $1.0 \times 3.0 \text{ mm}^2$  rectangular  $0.5 \text{ mm}$  thick bars and single crystals in the form of  $20\text{-}30 \text{ }\mu\text{m}$  thick  $1.0 \text{ mm}$  square wafers of wafers of  $\text{YBa}_2\text{Cu}_3\text{O}_{7-x}$ ,  $\text{Bi-Ca-Sr-Cu-O}$ , and  $\text{Ti-Ca-Ba-Cu-O}$ . Measurements included current-voltage characteristics of such junctions at  $4.2 \text{ K}$  without an external microwave field and in a  $72.9 \text{ GHz}$  microwave field producing a Shapiro effect (shelf within a periodic

segment segment of the current-voltage curve), temperature dependence of the critical current and of the electrical resistance  $R_n$  in the normal state, also temperature dependence of the  $I_0 R_n$  product ( $I_0$  - current differential ranging from deficiency at very low temperatures to excess at higher temperatures with zero crossover at some temperature below  $T_c$  and returning to zero at the critical temperature  $T_c$ ). The results indicate formation of a semiconductor layer on the cleavage surface, even at as low as liquid-helium temperatures. The temperature dependence of the electrical resistance in the normal state indicates a behavior like that of doped semiconductors, the presence of such a barrier layer moreover causing the temperature dependence of the critical current to become anomalous with one or several maxima. On the basis of the experimental data and in accordance with the B-C-S theory is constructed an S-N-I-N-S model of such junctions with resonance percolation trajectories through the barrier, the classical S-N-S ("dirty" limit) and S-I-S models not being adequate except for description of only very few of these junctions and narrowing of the energy gap, whether by the proximity effect or by the presence of magnetic impurities, needing to be accounted for. The authors thank M.Yu. Kupriyanov, K.K. Likharev, and A.V. Zaytsev for fruitful discussion of the results. Figures 9; references 17.

### High-Temperature Quantum Interferometer

927J0029B Kharkov FIZIKA NIZKIKH TEMPERATUR in Russian Vol 17 No 6, Jun 91 pp 790-792

[Article by V. V. Kartsovnik, P. P. Pavlov, V. A. Pavlyuk, and Yu. A. Tavrinn, Institute of Low-Temperature Engineering Physics, UkSSR Academy of Sciences, Kharkov, N. Ye. Khlebova and A. K. Shikov, All-Union Scientific Research Institute of Inorganic Materials, USSR Academy of Sciences, Moscow]

UDC 538.945

[Abstract] A high-frequency superconducting quantum interferometer has been designed for operation at a  $77 \text{ K}$  temperature and accordingly built with a high- $T_c$  superconductor material,  $\text{YBa}_2\text{Cu}_3\text{O}_{7-x}$  ceramic. This material was produced by modification of the conventional "three phases method" so as to include homogenization of the initial  $\text{Y}_2\text{O}_3 + \text{BaCO}_3 + \text{CuO}$  powder mixture in an air stream at a temperature within  $900\text{-}920^\circ\text{C}$  for  $10\text{-}15 \text{ h}$  prior to compaction and subsequent sintering at a temperature within  $900\text{-}940^\circ\text{C}$  for  $20\text{-}30 \text{ h}$ . The product was comminuted into powder and the latter again compacted for another sintering operation, this process being repeated a few times prior to annealing of the final product at various temperatures within the  $400\text{-}600^\circ\text{C}$  range for  $30\text{-}40 \text{ h}$  in an oxygen stream under a pressure of  $1 \text{ atm}$  and its subsequent cooling at a rate certain to yield a ceramic material consisting of the 123-phase only ( $13\pm 0.3 \text{ wt. percent Y}$ ,  $42.0\pm 0.8 \text{ wt. percent Ba}$ ,  $28.8\pm 0.4 \text{ percent Cu}$ , oxygen index  $6.90\text{-}6.92$ , density  $5.35$

$\text{g/cm}^3$ ) with a critical superconducting transition temperature  $T_c = 90$  K within a  $\Delta T = 1.2$  K wide fluctuation range and with a critical current density of approximately  $200 \text{ A/cm}^2$  at  $77$  K. The interferometer, a  $5 \text{ mm}$  thick and  $3 \text{ mm}$  wide ring with a single hole  $1 \text{ mm}$  in diameter, includes  $0.1 \text{ mm}$  long and  $0.2 \text{ mm}$  wide bridge. A weak Josephson link has been formed by high-voltage discharge treatment of this bridge. The performance characteristics of this interferometer under excitation at a  $10 \text{ MHz}$  high frequency at a  $77 \text{ K}$  temperature are:  $2\pi I_c/\Phi_0 = 2$  ( $I_c$  - critical current for weak link,  $\Phi_0$  - quantum of magnetic flux), flux resolution  $10^{-4} \Phi_0/\text{Hz}^{0.5}$  corresponding to a  $10^{-28} \text{ J/Hz}$  energy resolution, and magnetic field period  $2.5 \times 10^{-9} \text{ T}$  corresponding to a  $2.5 \times 10^{-13} \text{ T/Hz}^{0.5}$  field resolution in the presence of white noise. Excitation at a  $100 \text{ MHz}$  frequency is made feasible by installation by connecting the interferometer tank circuit to the high-frequency amplifier through a coaxial cable of half-wave length at  $100 \text{ MHz}$ . In this case the interferometer had a  $Q_0$ -factor of approximately  $50$  and a  $k \approx 0.2$  coefficient of coupling to the quantization circuit. Its flux resolution is then  $8 \times 10^{-4} \Phi_0/\text{Hz}^{0.5}$  corresponding to a  $6.4 \times 10^{-29} \text{ J/Hz}$  energy resolution and its field resolution is  $2 \times 10^{-13} \text{ T/Hz}^{0.5}$  with the same magnetic field period as before. Figures 1; references 3.

#### Anomalous Thermodynamic Characteristics of S-N Superlattice

927J0021C Moscow PISMA V ZHURNAL  
EKSPERIMENTALNOY I TEORETICHESKOY  
FIZIKI in Russian Vol 53 No 10, 25 May 91  
pp 503-507

[Article by A. I. Buzdin and A. Yu. Simonov, Moscow State University imeni M. V. Lomonosov, V. P. Damjanovich, Department of Natural and Mathematical Sciences at Titograd University (SFR of Yugoslavia)]

[Abstract] A superstructure consisting of alternating superconductor (S) and normal (N) monolayers is considered and its properties are analyzed on the basis of the Bulaevskii-Zyskin model (PHYSICS REVIEW Vol 42B, 1990), with Cooper pairing in the S-layers only and a skip interval between adjacent layers smaller than the Fermi energy  $E_F$ . Such a system is described by a Hamiltonian which includes the creation operator  $a_{i\sigma}^\dagger(p)$  referred to an electron with momentum  $p$  and spin  $\sigma$  within a layer  $i$  of the  $n$ -th unit cell consisting of S and N layers ( $i=1$  referring to an S-layer,  $i=-1$  referring to an N-layer) and the energy difference  $\xi(p) = E(p) - E_F$ , assuming for simplicity the same dispersion law for electron energy  $E(p)$  in S and N layers. An exact solution is then obtained for both normal and anomalous Green's functions. A larger skip interval  $t$  between S and N layers, signifying a stronger influence of an adjacent N-layer, means a lower critical temperature  $T_c$  but also a narrower energy gap  $\Delta$ . An integral equation is given for the ratio  $\Delta_c$ , its dependence on the ratio  $t/T_c$  having been evaluated numerically on this basis. Its value differs from  $\Delta(0)/T_c = 1.76$  at  $t=0$  according to the BCS theory, the

difference increasing as  $t$  increases. A relation is then established between  $\Delta(0)$  and a measurable quantity, namely the density of states  $\rho_i$ , readily determined in a tunnel experiment. The dependence of  $\rho_i(E)$  in S-layers and in N-layers on  $E/T_c$  has also been evaluated numerically for the case of gapless superconductivity, with the magnitude of the skip interval varied from  $t=0.2\Delta(0)=0.36T_c$  to  $t=\Delta(0)=2.2T_c$ . This dependence contains singularities which shift toward higher energy  $E$  as the skip interval  $t$  increases. The singularity at  $E=\Delta/2$  is almost the same in S-layers and N-layers. The singularity in the  $E > \Delta$  range is a  $\rho_i$  jump at  $E=\Delta=[4t^2+\Delta^2/2+(4t^2\Delta^2+\Delta^4)^{1/2}]^{1/2}$ , higher in S-layers than in N-layers. The singularity at  $E=\Delta$  is a  $\rho_i$  jump, higher in S-layers than in N-layers, its magnitude decreasing as the skip interval  $t$  increases and a second jump occurring at  $E=[(4t^2+\Delta^2/2+(4t^2\Delta^2+\Delta^4/4)^{1/2})]^{1/2}$  when  $t < 0.25\Delta$ . Tunnel measurements can thus yield values of  $\Delta_c$  much higher than its standard value according to the BCS theory. The results of this analysis apply also to high- $T_c$  superconductor structures, qualitatively if not quantitatively, even though the presence of many S and N layers with different skip intervals between them precludes a gapless superconductivity. The authors thank M.Yu. Kupriyanov and Ya.T. Ponomarev for discussing the results. Figures 4; references 7.

#### Electron Paramagnetic Resonance in (Er,Y)-Ba-Cu-O System

927J0041A Kharkov FIZIKA NIZKIKH  
TEMPERATUR in Russian Vol 17 No 5, May 91  
pp 637-643

[Article by A. G. Anders, S. V. Volotskiy, A. I. Zvyagin (deceased), and N. M. Charkovskaya, Institute of Low-Temperature Engineering Physics, UkSSR Academy of Sciences, Kharkov]

UDC 538.945

[Abstract] An experimental study of electron paramagnetic resonance in  $\text{Er}_{1-x}\text{Ba}_2\text{Cu}_3\text{O}_y$  ceramics with a wide range of Er concentrations ( $0.03 \leq x \leq 1$ ) and in  $\text{ErBa}_2\text{Cu}_3\text{O}_y$  ( $x=1$ ) single crystals was made, the EPR spectra being measured with these materials in both normal and superconducting states. Ceramics were produced according to the standard technology from  $\text{Y}_2\text{O}_3$ ,  $\text{Er}_2\text{O}_3$ ,  $\text{BaO}_2$ , and  $\text{CuO}$ , with  $\text{Er}_2\text{O}_3$  added in amounts yielding its desired concentration. Ceramic material was obtained by synthesizing the mixture of oxides at  $940^\circ\text{C}$  in air over a period of 6 h. The ceramic was comminuted into powder the latter was sifted. Its fine fraction of the  $8 \mu\text{m}$  average grain size was mixed with liquid paraffin and heated again to  $940^\circ\text{C}$  in air, after the paraffin was let thicken in a magnetic field of about  $4 \text{ kOe}$  intensity for the purpose of preorienting the powder micrograins prior to compaction. Transformation into the tetragonal phase was effected by quenching the ceramic from this temperature in liquid nitrogen. Single crystals in the form of plates up to  $0.1 \text{ mm}$  thick and up to  $1 \times 2 \text{ mm}^2$

large were produced by spontaneous solidification of a melt with a stoichiometric  $\text{Er}:\text{Ba}:\text{Cu} = 1:6:12$  content. Their transformation into the tetragonal phase was also effected by quenching in liquid nitrogen. The critical temperature of transition from normal to superconducting state was 85 K or close to it. The spectra of electron magnetic resonance were measured with a radio spectrometer which included a high-frequency channel adjustable for operation at 4 mm band and 8 mm band wavelengths in the 4 mm band, in the magnetic field of about 50 kOe intensity generated by a superconducting solenoid. All measurements were made at 4.2 K temperature. All spectra revealed the presence of  $\text{Er}^{3+}$  ions. On the basis of the experimental data have been calculated the g-factor and the width of the resonance line, also the Néel temperature  $T_N = 0.52$  K. The thus obtained values of the g-factor agree with those for an  $\text{Er}^{3+}$  ion in a slightly distorted cubic crystal field, the  $\text{Y}^{3+}$  ion which replaces an  $\text{Er}^{3+}$  ion in the  $\text{Er}_x\text{Y}_{1-x}\text{Ba}_2\text{Cu}_3\text{O}_y$  lattice being surrounded by O(2) and O(3) oxygen ions in the corners of a rectangular prism and the local surrounding of a remaining  $\text{Er}^{3+}$  ion being correspondingly distorted as the oxygen content increases from  $y = 6$  ( $\text{ErO}_6$ ) to  $y = 7$  ( $\text{ErO}_7$ ) or during transition from tetragonal to rhombic symmetry. In an axial magnetic field, moreover, the  $\text{Er}^{3+} I_{15/2}$  ground state splits into eight Kramers doublets. The width of resonance line is found to depend on the Er concentration, indicating an exchange interaction in the rare-earth subsystem comparable in strength with dipole-dipole interaction. The results reveal that resonance absorption of  $\text{Er}^{3+}$  ions occurs in all these materials, whether in the normal or superconducting state, no matter what the Er concentration is within the given range. Figures 3; references 17.

#### Formation of 2234-Phase in Bi-Sr-Ca-Cu-O Films Doped With Pb and Sb

927J0041B Kharkov FIZIKA NIZKIKH  
TEMPERATUR in Russian Vol 17 No 5, May 91  
pp 652-655

[Article by L. S. Palatnik, A. L. Toptygin, V. V. Prytkin, V. P. Gordiyenko, and N. V. Zubar, Kharkov Polytechnic Institute imeni V. I. Lenin]

UDC 538.945

[Abstract] An experimental study of Bi-Sr-Ca-Cu-O films doped with Sb alone or with Sb and Pb was made concerning their structure, electrical properties, and superconducting transition. Four groups of 5-10  $\mu\text{m}$  thick films were synthesized from mixtures containing respectively  $\text{Bi}_{1.9}\text{Sb}_{0.1}\text{Sr}_2\text{Ca}_3\text{Cu}_4$ ,  $\text{Bi}_{1.7}\text{Sb}_{0.3}\text{Sr}_2\text{Ca}_3\text{Cu}_4$ ,  $\text{Bi}_{1.6}\text{Sb}_{0.3}\text{Pb}_{0.1}\text{Sr}_2\text{Ca}_3\text{Cu}_4$ ,  $\text{Bi}_{1.6}\text{Sb}_{0.1}\text{Pb}_{0.3}\text{Sr}_2\text{Ca}_3\text{Cu}_4$ . They were synthesized in three stages under a vacuum of 0.1 mPa, beginning with evaporation of the components by electric resistance or

induction heating and subsequent condensation of the compound vapor on MgO single crystals. The temperature of the MgO substrates in this process was varied over the 150-400°C range, the reactor chamber having been vacuumized by means of a diffusion pump with a nitrogen trap. The chamber was then filled with pure oxygen at temperatures within 550-600°C only, for a preliminary 30-300 min long annealing of the films "in situ". Upon extraction from this chamber, the films were twice annealed in an atmosphere containing oxygen, the first time at temperatures within 880-900°C for 5-10 min and the second time at temperatures within 840-860°C for 30-300 min. Structural examination of the films was done under an REM-200 scanning electron microscope and in a DRON-2 x-ray diffractometer with a  $\text{FeK}_\alpha$ -radiation source. Their chemical composition was monitored in a LINK 860/500 x-ray microanalyzer. Their electrical resistance was measured by the current-voltage method at temperatures covering the 77-300 K range and the superconducting transition temperature was then determined by extrapolation of the resistance curves to  $R = 0$ . Diffractograms recorded after the first heat treatment revealed a polycrystalline polyphase structure with random grain orientations and with amorphous inclusions. The principal component was the 2212 phase, its high electrical resistance having a semiconductor-like temperature dependence with no transition to the superconducting state at 77 K. Diffractograms recorded after a second heat treatment at 860°C revealed a 2212 phase grown epitaxially with the (001) plane parallel to the (100) plane in the MgO substrate, this phase having an electrical resistance much lower than that of the other 2212 phase and constant over the entire temperature range till transition to the superconducting state with a critical temperature within 79-77 K. Diffractograms recorded after a second heat treatment at 845-850°C revealed a new phase along the 2212 phase, namely the 2234 phase with four Cu-O layers in the tetragonal lattice. Superconducting transition in films doped with Sb alone and containing the 2234 phase was found to begin at 120 K, without traces of the 2223 phase, and to end at a temperature within 82-80 K. Superconducting transition in these films thus begins at a temperature much higher than in pure 2212-phase films, where it begins at temperatures ranging from 110 K to 90 K, but extends over a wider temperature band. Even a small amount of the 2234 phase in a film was found to change the temperature dependence of the electrical resistance into a metal-like one with a much larger temperature coefficient. This new phase was also found to be sensitive to the heat treatment temperature, readily breaking up when that temperature was raised by as little as 5-10°C. Superconducting transition in films doped with Sb and Pb was also found to begin at a temperature higher than in pure 2212-phase films, but not as high as 120 K. Formation of the 2234 phase is thus evidently facilitated by doping Bi-Sr-Ca-Cu-O films either with Sb alone or with Sb and Pb. Figures 2; references 8.

**Microwave Absorption by Type-II Superconductors in Magnetic Field**

927J0041C Kharkov FIZIKA NIZKIKH TEMPERATUR in Russian Vol 17 No 5, May 91 pp 656-659

[Article by S. N. Lukin, O. P. Teslya, and G. A. Tsintsadze, Institute of Cybernetics, GSSR Academy of Sciences, Tbilisi]

UDC 538.045

[Abstract] An experimental study of microwave absorption by type-II superconductors such as niobium and  $T_c$  ceramics in strong magnetic fields was made, its purpose being to determine the field dependence of absorbed microwave power. Powder of Y-Ba-Cu-O ceramic obtained by grinding large pieces in an agate mortar was sifted for extraction of a homogeneous grain fraction. Powder of metallic niobium was obtained by machining an ingot and sifting the chips for extraction of a homogeneous size fraction. For measuring the power of absorbed microwaves in the 4 mm band was used an EPR video spectrometer operating in this wave band and an EPR radio spectrometer with an oversize cavity, a specimen of superconductor powder suspended in paraffin lining the bottom of that cavity in a layer of uniform thickness. The radio spectrometer operated in the direct-detection mode without magnetic modulation of the signal. An external magnetic field of up to 50 kOe was produced by a superconducting solenoid. The temperature of the superconductor layer was measured with a copper resistance thermometer. Resonance curves were recorded with the aid of a microwave bridge, in "change of bridge balance vs. solenoid current (magnetic field intensity)" coordinates. The field stabilization system was designed to allow for reversing the direction of the solenoid current and thus also of the magnetic field intensity vector so that the magnitude of the latter would pass through zero. Measurements at 4.2 K revealed microwave absorption by Y-Ba-Cu-O ceramic due to resonance of Cu ions along a much weaker off-resonance microwave absorption in the magnetic field. As the temperature of the superconductor layer was raised, this off-resonance absorption was found to become stronger and dependent on the field intensity. Within the 88-92 K temperature range the off-resonance absorption signal became comparable in magnitude with the signal from Cu ions and above 92 K it ceased to depend on the field intensity. Microwave absorption by metallic Nb was found to follow an analogous trend at 4.2 K, with a resonance curve being symmetric relative to the zero field intensity point and with absorption saturating at a field intensity above 9.5 kOe. At higher temperatures the off-resonance absorption by metallic Nb was found to become strongly and monotonically dependent on the field intensity, even where this microwave absorption by Y-Ba-Cu-O ceramic ceased to be field-dependent. The field dependence of microwave

absorption is hypothetically attributed not only to magnetic creep but also to formation and migration of vortices with eyes in the normal state. Measurements made without an external magnetic field revealed, moreover, a strongly nonlinear over the 4.2-92 K range temperature dependence of microwave absorption by both Y-Ba-Cu-O ceramic and metallic Nb in absence of a magnetic field. Figures 3; references 5.

**Raman Spectroscopy of  $\text{CsMnCl}_3 \cdot 2\text{H}_2\text{O}$  Crystal**

927J0041D Kharkov FIZIKA NIZKIKH TEMPERATUR in Russian Vol 17 No 5, May 91 pp 630-636

[Article by V. P. Gnezdilov, V. V. Yermenko, V. S. Kurnosov, and V. I. Fomin, Institute of Low-Temperature Engineering Physics, UkSSR Academy of Sciences, Kharkov]

UDC 535.375

[Abstract] An experimental study of catenulate quasi-one-dimensional antiferromagnetic  $\text{CsMnCl}_3 \cdot 2\text{H}_2\text{O}$  crystals was made involving Raman spectroscopy for an analysis of their fundamental lattice vibrations, these crystals having an orthorhombic structure and being transparent with a weak pink tint. Specimens in the form of  $3 \times 5 \times 7 \text{ mm}^3$  large right parallelepipeds were cut from crystals with a well defined habit and their surfaces then polished to an optical-grade finish. They were placed in an optical cryostat containing superfluid He-4 and then excited by an Ar<sup>+</sup>-laser with about 200 mW of 488.0 nm radiation for Raman scattering in the standard 90° configuration. Instrumentation for recording the Raman spectra included a "Ramanor - U 1000" double monochromator and a single-channel photon counter with an appropriately cooled photomultiplier, this instrumentation operating automatically with control by a personal computer. Also the speed of sound in these crystals was measured, by the Mandelshtam-Brillouin scattering method. Considering that a unit cell of such a crystal has a  $D_{2h}^8$  (Pcca) space group symmetry and can be represented as two or more chains of  $\text{MnCl}_4\text{O}_2$  octahedra along the a-axis, connected by hydrogen bonds and surrounded by Cs ions, an analysis based on group theory yields six presumably low-frequency vibration modes: acoustic, lattice, and chain vibrations,  $\text{H}_2\text{O}$  rotational,  $\text{H}_2\text{O}$  deformational, and  $\text{H}_2\text{O}$  valence vibrations. They include rotations of an  $\text{MnCl}_4\text{O}_2$  octahedron as a whole ( $A_g + B_{1g} + 2B_{2g}$ ), translations of a chain as a whole ( $B_{1g} + B_2 + B_{3g}$ ), and translations of Cs ions ( $A_g + B_{1g} + 2B_{2g} + 2B_{3g}$ ), motions of hydrogen atoms having been ignored. The recorded spectra, containing very faint lines as well as very intense lines, confirm that all these modes have been excited and indeed within the  $30\text{-}100 \text{ cm}^{-1}$  frequency range. The spectra reveal also an anomalously long mean life of low-frequency phonons, as manifested by small half-widths of the corresponding lines, even when recorded at room temperature. The higher-frequency vibration modes within the  $100.6\text{-}350$

cm<sup>-1</sup> range are evidently internal chain vibration modes of the Mn-Cl bond and Mn-O bond "elongation-contraction" type. The authors thank I.S. Kachur for supplying the crystals and Yu.V. Cherepakha for measuring the speed of sound in them. Figures 2; references 12.

### Microwave Absorption by High-T<sub>c</sub> Superconductor Ceramic in Magnetic Field

927J0024C Leningrad FIZIKA TVERDOGO TELA in Russian Vol 33 No 4, Apr 91 pp 1226-1237

[Article by V. V. Kveder, M. R. Mkrtchyan, and A. I. Shalynin, Institute of Solid-State Physics, USSR Academy of Sciences, Chernogolovka (Moscow Oblast)]

UDC 291.19.29.26

[Abstract] The anomalously strong absorption of microwave power by high-T<sub>c</sub> superconductor ceramic in magnetic fields at temperatures below the critical one is analyzed theoretically, for an interpretation of the results of experiments performed with YBa<sub>2</sub>Cu<sub>3</sub>O<sub>6+x</sub> ceramic and single crystals at temperature down to 30 K and at 1.4 K. Microwave measurements were made inside a rectangular cavity with a high-frequency ( $\omega = 9300$  MHz) magnetic field  $H_{\omega}$  and a parallel to it constant one  $H_0$ , a specimen having been placed in a loop of the  $H_{102}$  cavity mode. The resonance curve of the cavity having been obtained by measurements, its half-width was used for calculation of the absorbed power. Absorption measurements were also made at low frequencies covering the 0.1-10 kHz range, with the specimen inside one of two receiver copper coils connected in series-opposing inside a solenoid generating such a low-frequency magnetic field and connected to a lock-in amplifier outside. The c.m.f.'s then induced in these coils in phase quadrature

were measured for the purpose of determining both real and imaginary parts of the magnetic susceptibility  $\chi$  of the specimen, the imaginary part  $\chi''$  then being used for calculating the absorbed power  $P = \omega H_{\omega}^2 \chi''/2$  and the real part  $\chi'$  for calculating the area of the specimen completely shielded from the high-frequency magnetic field by supercurrents. Both the temperature dependence of microwave power absorption in a constant magnetic field and its dependence on the intensity of the high-frequency magnetic field  $H_{\omega}$  are evaluated numerically on the basis of the authors' as well as other available experimental data and on the basis of theoretical relations applicable to a granular ceramic material as an array of spherical grains closely packed except for a gap between two of the rows, assuming that the mean "magnetic width" of superconducting transition in this model is equal to the field penetration depth plus the average area of nonsuperconducting interstices. In addition to that is also evaluated the dependence of microwave power absorption in both magnetic fields on the intensity  $H_0$  of the constant and static one, the results confirming the existence of a narrow characteristic "weak-field" absorption line which corresponds to an increase of  $\chi''$ . When the intensity of this constant magnetic field is varied, the dependence of absorbed microwave power on that intensity has been found to be an oscillatory one. The pattern of microwave power absorption as a function of time and its temperature dependence in both high-frequency and constant magnetic fields fits not only qualitatively but also quantitatively the model of absorption in long and highly nonhomogeneous Josephson junctions. Application of a "pumping" second microwave field of another frequency and sufficiently high amplitude has, moreover, been found to induce in such junctions a current larger than the critical one and the ceramic material to respond to the primary high-frequency magnetic field as if the critical current were zero. Figures 12; references 16.

**Speed of Sound in Primary Normal Liquid Alcohols**

927J0062A Moscow *TEPLOFIZIKA VYSOKIKH TEMPERATUR* in Russian Vol 29 No 4, Jul-Aug 91 pp 710-716

[Article by T. S. Khasanshin, Moscow Institute of Technology]

UDC 534.2:547.26

[Abstract] Published data on the speed of sound in liquid primary normal alcohols at elevated parameters - 273-473K and a pressure of  $\leq 100$  MPa - are reviewed and the behavior patterns of the speed of sound in a homological series of N-alcohols are examined. Acoustic properties of little-known representatives of the series are predicted and refined while correlation equations which reflect the dependence of acoustic properties on the number of carbon atoms in the alcohol molecule, temperature, and pressure are derived. A procedure for calculating the speed of sound in these alcohols is proposed and calculations demonstrate that it reflects the initial data on the speed of sound with an error not exceeding that of the experiment and is suitable for forecasting acoustic properties in a series starting with  $C_4$  in the domain of liquid state. A comparison of analytical and experimental data at a 433.15K temperature shows a discrepancy of less than 0.15 percent. It is noted that if reliable data on the speed of sound in  $C_4$ - $C_{12}$  alcohols are available, there is no need for systematic direct measurements of the speed of sound in alcohols with more than 12 carbon atoms in the temperature and pressure ranges under study. Figures 1; tables 3; references 14: 11 Russian, 3 Western.

**Thermodynamic Functions of Three-Dimensional Ising Model Near Phase Transition Point Allowing for Scaling Corrections. II.  $TT_c$  Case**

927J0052A Moscow *TEORETICHESKAYA I MATEMATICHESKAYA FIZIKA* in Russian Vol 87 No 3, Jun 91 pp 434-455

[Article by M. P. Kozlovskiy, I. V. Pylyuk, I. R. Yukhnovskiy, Lvov Statistical Physics Branch of the Theoretical Physics Institute at the Ukrainian Academy of Sciences]

[Abstract] An original method of calculating the statistical sum of three-dimensional model systems near the phase transition point which makes it possible to compute the thermodynamic and structure functions near  $T_c$  including confluent corrections, is discussed. The method is extended to the case of  $TT_c$ ; the universal character of critical amplitudes is investigated and their dependence on microscopic Hamiltonian is examined. The behavior of the system in the domain of  $TT_c$  is described allowing for the two principal fluctuation processes occurring near the second-kind transition point - the former describes short-wave fluctuations and is referred to as the critical condition (KR); the latter is a long-wave fluctuation process of the spin moment density and is referred to as the inverse Gaussian condition (IGR). It is shown that critical amplitude can be represented as a universal term and a nonuniversal multiplier which depends on the Hamiltonian's microscopic parameters. Expressions are derived for certain critical amplitude combinations and the contribution of scaling corrections to the heat capacity of the system is estimated. If only the KR contribution is taken into account, negative heat capacity values are produced; the inclusion of the IGR contribution stabilizes the system. Figures 6; tables 9; references 27: 9 Russian, 18 Western.

**END OF**

**FICHE**

**DATE FILMED**

4 May 1992